FUNDAMENTALS OF A METAL SURFACE IMAGING SYSTEM BASED ON LASER-OPTIC PRINCIPLES

MURAT BEKTAŞ

MAY 2009

FUNDAMENTALS OF A METAL SURFACE IMAGING SYSTEM BASED ON LASER-OPTIC PRINCIPLES

A THESIS SUBMITTED TO
THE GRADUATE SCHOOL OF NATURAL AND APPLIED SCIENCES
OF
MIDDLE EAST TECHNICAL UNIVERSITY

BY

MURAT BEKTAŞ

IN PARTIAL FULFILLMENT OF THE REQUIREMENTS
FOR
THE DEGREE OF MASTER OF SCIENCE
IN
PHYSICS

MAY 2009

Approval of the thesis:

FUNDAMENTALS OF A METAL SURFACE IMAGING SYSTEM BASED ON LASER-OPTIC PRINCIPLES

submitted by **MURAT BEKTAŞ** in partial fulfillment of the requirements for the degree of **Master of Science in Physics Department, Middle East Technical University** by,

Prof. Dr. Canan Özgen _____
Dean, Graduate School of **Natural and Applied Sciences**

Prof. Dr. Sinan Bilikmen _____
Head of Department, **Physics**

Prof. Dr. Hakan Altan
Supervisor, **Physics Dept., METU** _____

Examining Committee Members:

Prof. Dr. Sinan Bilikmen _____
Physics Dept., METU

Assoc.. Dr. Hakan Altan _____
Physics Dept., METU

Prof. Dr. Bülent Akınoğlu _____
Physics Dept., METU

Dr. Halil Berberoğlu _____
Physics Dept., METU

Asist. Prof. A. Behzat Şahin _____
Electrical and Electronics Eng. Dept., METU

Date: 13.05.2009

I hereby declare that all information in this document has been obtained and presented in accordance with academic rules and ethical conduct. I also declare that, as required by these rules and conduct, I have fully cited and referenced all material and results that are not original to this work.

Name, Last name : Murat Bektaş

Signature :

ABSTRACT

FUNDAMENTALS OF A METAL SURFACE IMAGING SYSTEM BASED ON LASER-OPTIC PRINCIPLES

Bektaş, Murat

M.S., Department of Physics

Supvervisor : Instructor Dr. Hakan Altan

May 2009, 57 pages

The confocal laser-scanning microscope (CLSM), known simply as a confocal microscope, is an important instrument which allows us to observe an object or a surface in three-dimensions with confocal microcopy technique. The basic difference of confocal microscopy is detecting the in- focused light, while the out of focus light is blocked out by the help of a pinhole. By this optical dissection ability of confocal microcopy, CLSM provides the images of investigated object or the surface with higher resolution and contrast as against conventional microscopic systems. Various types of Laser Scanning confocal microscopes have been developed and due to its high resolution and contrast they have become an invaluable tool for investigations in many areas like biology and medicine. In addition to its wide range of use, confocal microscope can be used for detecting of possible defects on metal surfaces.

In this thesis our goal was to develop the analytical and theoretical back ground necessary for the successful completion of a laser/optic system coupled to a fiber bundle waveguide based on confocal scanning principles to effectively image a non-uniform, metal surface with speed and precision in order to assess any surface damage. In addition to this analysis we demonstrate a working confocal microscopy set-up and investigate the factors which affect the image quality by the experiments conducted in METU (Middle East Technical University) Laser Laboratory.

ÖZ

ÇEŞİTLİ METAL YÜZEYLERİN ÖLÇÜMÜNDE KULLANILICAK LAZER/OPTİK SİSTEMLERİNİN TEMELLERİ

Bektaş, Murat

Yüksek Lisans, Fizik Bölümü

Tez Yöneticisi : Öğr. Gör. Dr. Hakan Altan

Mayıs 2009, 57 sayfa

Eş odaklı Lazer Taramalı Mikroskop (EOLTM), daha basit bilinen adı ile eş odaklı mikroskop, eş odaklı mikroskopi tekniği ile objelerin ya da yüzeylerin üç boyutlu gözlemlenebilmesini sağlayan önemli bir aygıttır. Eş odaklı mikroskopinin en temel farkı; küçük bir deliğe sahip aparat yardımıyla odaklanmış ışığın algılanması ve odaklanmayan ışığın dışlanmasıdır. Bu küçük parçalara ayırıp görüntüleme becerisi sayesinde, EOTLM bize incelenen objenin ya da yüzeyin klasik mikroskopik yöntemlere kıyasla daha yüksek çözünürlük ve kontrast ile görüntülenebilmesini sağlamaktadır. Değişik tiplerde lazer taramalı eş odaklı mikroskoplar geliştirilmiş ve yüksek çözünürlük ve kontrast sağlaması sayesinde bu cihazlar, biyoloji ve tıp gibi bir çok alanda paha biçilmez araçlar haline gelmiştir. Bu geniş kullanım alanına ek olarak eş odaklı mikroskop, metal yüzeyler üzerindeki olası yüzey kusurlarının tespit edilmesinde kullanılabilir.

Bu tezde amacımız eğri metal yüzeylerin görüntülenebilmesini sağlayacak, frekans yönlendirici fiber demeti ile birleştirilmiş ve eş odaklı tarama tekniklerine dayanan bir lazer optik sistemin geliştirilebilmesi için gerekli analitik ve teorik inceleme ortaya koymaktır. Teorik analize ek olarak, ODTÜ (Orta Doğu Teknik Üniversitesi) Lazer Laboratuvarında kurduğumuz bir eş odaklı mikroskop düzeneğini çalıştırarak, görüntü kalitesini etkileyen faktörleri inceledik

ACKNOWLEGMENTS

I would like to thank to my supervisor Dr. Hakan ALTAN. I'm so grateful to him for his guidance and his support. I'm so glad to be his student and always remain grateful to him.

I also would like to thank to Dr. Halil BERBEROĞLU. He helped me a lot and shared his knowledge and experiences with me during this thesis study.

TABLE OF CONTENTS

LIST OF FIGURES

FIGURES

CHAPTER 1

INTRODUCTION

Various metals and metal parts are used in manufacturing and machine technologies. These range from aluminum and steel to precious metals such as gold and platinum. As the metals are worked on to obtain various machine parts (such as rifled bores) or pieces they can display various defects which may or may not affect their performance. To improve manufacture and quality control it is imperative that we can characterize these surface defects. Technologies based on magnification/eye imaging using endoscopic systems have been traditionally used to detect defects, such as bumps, burrs, marks and holes. To characterize these defects traditional methods have been to scan the surface using a stylus or point like metal tip and obtain a 3 dimensional profile [22,5]. While these systems are very accurate and can even scan at a resolution of less than 100nm, they are slow and are not suitable for a manufacturing environment where speed is a necessity.

Methods that use light sources to image the surface have gained much attention since they offer a low-cost alternative for such applications. When trying to image small scales microscope like systems are employed to obtain a high degree of resolution and contrast. Systems that utilize such sources generally obtain the profile of the metal surface by analyzing the reflected intensity of the light. The ultimate limit in resolution for these systems, not accounting for the lenses and other optics used, is the Rayleigh limit which is about half the wavelength of the light source [8-10,26]. Using near-field imaging techniques this limit can be further reduced [1]. Light sources utilized can be classified as coherent or non-coherent. Non-coherent sources such as white light, or a light bulb, have been used extensively. While they offer a cheaper method of profiling a surface, the capability of the system is limited

due to the power and incoherence of the source with the inability to study the surface due to phase changes upon reflection. Lasers, invented in the 1960s, have offered a more preferred method of illumination than the traditional white light source. Recently with advent of laser diodes the cost of laser systems has reduced dramatically making them applicable to manufacturing technologies. These lasers systems are able to emit from the visible to the infrared part of the electromegnatic spectrum and produce a much larger power output than one would obtain with a conventional white light source. Typical powers close to a watt are not uncommon and offer a cost effective alternative to image a surface with a high degree of resolution. In addition, since the light beam is coherent, phase changes can be applied in examining the 3 dimensional profile.

After the light source is implemented or selected, it has to be delivered onto the metal surface so that we can analyze the reflected light upon reflection. Traditional delivery methods involve coupling the light source through air and through a system of optics similar to that used in microscopes to deliver the beam onto a small field of view for high resolution imaging. Since lasers are being used more extensively in these imaging systems, optical fibers can be used as well to deliver the beam onto the area to be imaged. The use of fibers allows for imaging confined spaces or the insides of tube like surfaces which would be impossible otherwise with any other of the aformentioned methods. Imaging systems which utlize fibers are extensively employed in the medical and industrial communities. The field has adavanced far enough so that the dispersive properties of the fiber is used to manipulate the beam in oreder to get a higher degree of resolution upon imaging such are techniques used in optical coherence tomography systems (OCT) [23].

To effectively understand the principles of imaging a plane (metal) with a high degree of resolution using a laser as a source of illumination one needs to understand the effect of optics and other elements that are employed to achieve this goal. One method which is being used througout the microscopic imaging community is confocal scanning microscopy. Confocal scanning microscopy has offered the ability to not only image in two dimensions but also get depth information of the sample

being analyzed. This means that three dimensional imaging can be done to profile the surfaces of metal parts.

Finally, to analyze the image, the light reflected off the metal surface has to be detected using some sort of photodetector. Systems that employ white light sources generally detect the field through 2-dimensional detectors such as charged coupled device (CCD) cameras. These methods are fast but are limited due to 1: the power of the incoherent source and 2: The sensitivity of the detector. The use of lasers has eliminated the first problem but in order to increase sensitivity point detectors such as avalanche photodetectors (APDs) or photo multiplier tubes (PMTs) are being used readily. These detectors are far cheaper than CCDs and effectively reduce the cost of the system while increasing the complexity of the image acquisition considerably. Both hardware and special software are needed to scan the image when using point detectors. The hardware generally involves mirrors which you can use to scan the field of view in two dimensions. To obtain the image rapidly (often refererred to as video imaging or 30 frames per second imaging (30fps)), mirrors on galvonomoter controlled axes are used to scan at a needed fast rate. The software part has to do with combining all the point like data obtaing from the photodetector into a two dimensional and finally a three dimensional image to be analyzed by the user. The software has to be fast enough that it can analyze the images in real time, other wise you will need to buffer the data coming from the detector. All these issues contribute to the complexity of the imaging process and need to be analyzed systematically.

In this thesis, we will give a systematic analysis of the working principles behind obtaining images using confocal microscopy based scanning methods.

1.1 Microscopy

Different microscopic methods have been used for different needs of researchers. Mostly 2-Dimensional images and analysis can answer to researchers needs but when they need futher features like 3-dimensional analysis classical microscopic methods

are become awkward. A conventional microscope works well for thin specimens (i.e. less than 4μm). This is because the specimen is approximately 2-dimensional and thus all of it lies in the same focal plane. However, when dealing with a thick specimen, this resolution is lost in conventional microscopy. This is because only one thin slice through the specimen can be in-focus at any given time. The rest of the specimen (most of it) is out-of-focus resulting in an image that is mainly out-of-focus.

We need confocal microscopy because, in our research, we need to be able to microscopically analyze metal surfaces in order to gain quantitative information about the presence of any surface defects. This type of analysis is not possible with the use of conventional microscopy. Conventional microscopy gives us a projected and out-of-focus 2-dimensional (2D) image of a thick 3-dimensional (3D) object.

In a confocal scanning optical microscope (CSOM) either the object to be imaged or the source radiation must be scanned in order to build up the image point by point. Sample, objective, and beam scanning methods are techniques which allo for the image to be built up pixel by pixel. Conventional systems where sample scanning is used typically takes of the order of 10 s per frame, dependent on the area to be scanned. All the instruments used in a CSOM scheme can be and have been improved upon, allowing the optical system to be adjusted to produce different imaging configurations. An alternative method of image formation is to scan the objective lens. This technique is seldom used because it is difficult to maintain uniform illumination across the field of view of the obejective [1].

The majority of commercial CSOMs [28] use some form of beam scanning, resulting in image formation typically much faster than that which could be obtained with sample scanning. In addition, because the scan is sectioned by the objective lens, the mechanical stress on beam scanning systems are less critical than those systems which utilize sample scanning. There are various methods for beam scanning. The simplest form is to raster scan (scan across) the pinhole, or replace the pinhole with a single-mode optical fiber and scan across the fiber. A faster method is to scan the

optical beam in transmisson and reflection using a galvanometer mirror. One could also use an acoustooptic cell for a rapid scan in at least one axis. Imaging systems which require at least 30fps generally will replace the single pinhole with a Nipkow disk, which contains a patterned array of a large number of pinholes. Many of these methods are capable of producing real-time images at video frame rates. All these scanning techniques have been employed in various forms of commercial confocal microscopes [1].

The major advantage of the CSOM over a standard optical microscope is that due to optical sectioning the defocused part of the image disappears, where for a standard optical microscope it will become blurred. In the past, before the invention of the confocal microscope, it was necessary to slice the material into thin layers and mount each slice onto a microscope slide to obtain adequate cross-sectional images. A standard transmission microscope was usually used to observe these thin cross-sections. Another advantage of the CSOM is that due to its use of depth resolution to eliminate reflections from glass slides and coverslips, it is possible to observe many types of samples wi1thout slicing them into thin sections. In other words, when examining relatively thick materials, a CSOM reflection microscope has the advantage that details of an image will not be obscured by glare from layers in front of or behind of the region of interest [1].

One final advantage is the use of CSOMs with fluorescent imaging applications, where the sample is illuminated at one wavelength exciting the fluorescent material, causing it to fluoresce at a longer wavelength than that of the incident light. The sample is imaged through a filter which passes only the longer wavelength radiation (fluorescense). Elimination of out-of-focus planes from the image removes the blurred fluorescent signal from regions of the sample where the beam is not as well focused [1].

The source of illumination is important and needs to be addressed for these types of applications. The function of the illuminating source in typical CSOMs is to provide

a stable source of spatially coherent light for the microscope. The confocal scanning laser microscope (CSLM) uses a laser, pinhole, and beam expander to achieve this goal. Lasers are common sources for CSOMs because they provide an inexpensive bright monochromatic coherent light source. In fluorescense applications, a single-frequency source simplifies the use of the barrier filters and dichroic mirrors required for the separation of the excitation and fluorescent beams. Furthermore, many fluorescent dyes require significant pump power to generate an adequate response for fluorescent imaging, thus requiring the use of lasers [2].

When selecting a laser for use in a CSLM, one has to consider specifications such as its mode structure, intensity, directivity, and wavelength stability. Typically it is preferred that the laser should have its output in a TEM_{00} mode. A pure TEM_{00} output allows a beam expander to illuminate the objective lens uniformly without the use of a pinhole in the illumination path to form a spatial filter. In such a system the point source criterion for a CSOM can be fulfilled without the use of a pinhole because the light appears to originate from a point source at infinity. In the instance when the laser beam has imperfections, it can be "cleaned up" by focusing it onto a pinhole somewhat smaller than the focused beam spot size [1,2,24].

The power stability of the laser is probably the most important parameter because a change in the source power can be interpreted as a change in reflected intensity from the sample. In addition to power stability, lasers are specified by their directivity. The directivity is a critical factor when a spatial filter, or pinhole, is used in the beam expander. Instability in the pointing direction of the laser will be converted into intensity changes of the light from the sample. When a pinhole is not used in the illumination system, then changes due to the pointing instability can change the apparent position of the spot on the sample. In most commercial systems the change of position is generally small compared with the spot size of the beam on the sample[2].

Wavelength stability is less important than intensity or pointing stability in CSLM systems. Since most applications are not wavelength sensitive, a small change in the source wavelength will have little or no affect on the image. Many different types of lasers have been used in CSLMs. Helium-neon gas lasers have been a good choice because they are not only inexpensive and reliable but also can be amplitude stabilized for precise measurement applications. In addition, they are available in a variety of wavelengths. Another alternative is a diode laser which is not only stable and but also inexpensive. Care must be taken to eliminate feedback of the reflected beam into the laser, which can cause intensity fluctuations. Argon lasers that provide green or blue light are particularly useful sources for fluorescence imaging, due to their shorter wavelength and higher average power. HeCd lasers are typically not used because of problems with stable output power and pointing stability[1,2,24].

In reflection mode microscopes for imaging in materials science applications, a broadband mercury or xenon arc lamp, is preferred as an illumination source. Broadband illumination reduces interference effects of the light reflected from different layers of the sample, which can significantly reduce the quality of the image. This type of illumination is especially important when imaging integrated circuits that are composed of multiple dielectric layers particularly on reflecting substrates [2].

Broadband sources such as arc lamps have several advantages compared to other types of broadband light sources such as filament lamps. They are compact, efficient, and have a high brightness so that they be easily focused onto the illumination pinhole. Furthermore, arc lamps have a much larger bandwidth. For example, light from a xenon lamp spans a region from about 230 nm to greater than 750nm. One potential disadvantage of imaging with a broadband light source is that chromatic aberration due to lenses and other optical elements will cause different focal planes on the sample to have different colors. This aberration can be beneficial in inspection applications where areas of the sample at different focus positions are easily distinguished by their different colors. However, in most metrology applications,

axial chromatic aberration will decrease the depth resolution and thus degrade the overall resolution of the microscope in the axial direction [2].

In addition to housing the light source, in a typical CSOM the illumination system should contain a set of lenses to focus the light onto a pinhole and then transmit the light from the pinhole to the rest of the optical system. The beam expander should also have a sufficient magnification in order to fill the pupil of the objective lens uniformly with the illuminating light. If the objective pupil is not uniformly filled, the decrease in light intensity near the edges of the lens will lower the effective numerical aperture of the lens and lower the system axial resolution [2].

1.2 What is a Confocal Misroscope? How Does It Work?

The confocal microscope is an important tool since it provide us images with increased resolution and contrast with respect to classical microscopic methods. A confocal microscope forms sharp images of a sample that would otherwise appear blurred when viewed with a conventional microscope. This is achieved by excluding most of the light from the sample that is not from the microscope's focal plane. The image has less fuzz and better contrast than that of a conventional microscope and represents a thin cross-section of the sample under study. Not only is it possible to observe fine details but it is also possible to build three-dimensional (3D) reconstructions of a volume of the sample by building up a series of thin slices taken along the vertical axis [3].

Confocal microscopy was invented by Marvin Minsky in 1955 while he was a Junior Fellow at Harvard University. His invention performed a point-by-point image construction by focusing a point of light sequentially across a specimen and then collecting the returning beam from the sample. This way, by illuminating a single point at a time, most of the unwanted scattered light that obscures an image when the entire specimen is illuminated was avoided. In addition, the light returning from the specimen passed through a second pinhole aperture that rejected rays that were not

directly from the focal point. The light rays that remained would then be detected by a photomultiplier and the image was gradually reconstructed using a long-persistence screen (a display full of phosphors that was excited). To build the image, the specimen was scanned by moving the stage rather than the beam of light. In this manner, the complexity of the system was avoided since a sensitive alignment of moving optics was not necessary. Instead of using stages attached to motors a 60 Hz solenoid was used to move the plat- form vertically and a lower-frequency solenoid was used to move it horizontally. The result was a frame rate of approximately one image every 10 sec.

The confocal microscope brings together the ideas of point-by-point illumination of the sample and rejection of the out-of-focus light. One downfall with imaging a point onto the specimen is that there are fewer emitted photons to collect at any given point in time. So to avoid building a noisy image each point must be illuminated for a long time to collect enough light to make a precise measurement. Correspondingly, this increases the length of time needed to create a point-by-point image. The solution to this problem is to use a light source with a very high intensity, which Minsky had done with a zirconium arc lamp. In the present day the choice is a laser, which has the additional benefit of being available in a wide array of wavelengths [3].

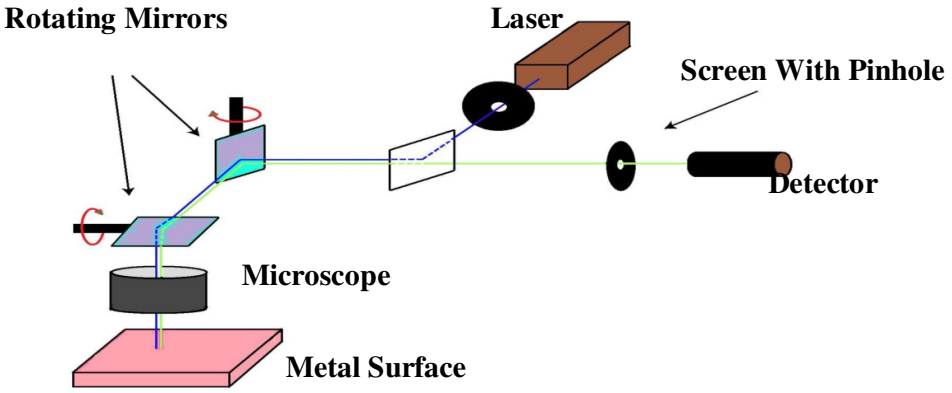

Figure 1.1 Basic setup of a confocal microscope. Light from the laser is scanned across the metal surface by the scanning mirrors.

In Fig. 1.1 the laser provides the intense source of illumination. The light reflects off a beamsplitter, which directs it to an assembly of vertically and horizontally scanning mirrors. These galvo motor-driven mirrors scan the laser across the sample. Contrary to this, Minsky's invention kept the optics stationary and instead scanned the sample by moving the stage back and forth in the plane perpendicular to the incident beam. Even though this was a slow method it does the following two major advantages:

- The sample is illuminated everywhere axially, rather than at different angles as in the case of the scanning mirror configuration. This reduces optical aberrations.

- The field of view can be made larger than that of the stationary objective by controlling the movements of the stage.

In Fig. 1.1 the sample is illuminated by the laser. The reflected light is descanned by the same mirrors that are used to scan the source beam from the laser and then passes through the beamsplitter. From here on, it is focused onto the pinhole. The light that passes through the pinhole is measured by a detector, typically a photomultiplier tube if the light passing through is very weak [REF 3].

In confocal microscopy, there is never a full image of the sample because at any point in time only one spatial point is observed. In order to visualize the image, the detector is attached to a computer, and appropriate software allows for the image to ve built up one pixel at a time. For a 512 x 512-pixel image, in commercial applications, this is typically done at a frame rate of 0.1– 30 Hz. The large range in frame rates depends on a number of factors.

The image created by the confocal microscope is of a thin planar section of the sample a method known as as optical sectioning. Out of plane unfocused light is ejected, resulting in sharper, both axially and laterally, better resolved images [3] Laser-based scanning confocal fundamentals (resolution, contrast, point spread

function) and image scanning & formation by experiment will be investigated in chapter 2 and chapter 3.

CHAPTER 2

RESOLUTION AND CONTRAST IN CONFOCAL MICROSCOPY

Imaging systems have been improved by new technological developments and reserachers desire to acquire more qualified images with the help of these improved imaging sytems. Image quality can be described mainly by two parameters which are resolution and contrast. All optical microscopes, including conventional widefield and confocal systems are limited in the resolution that they can achieve by a series of fundamental physical factors [11,16,20,24]. In a conventional optical system, resolution is restricted by the numerical aperture of optical components and by the wavelength of light, both incident (excitation) and detected (emission or reflected). The concept of resolution is closely related to contrast, and is defined as the minimum separation between two points that results in a certain level of contrast between them [20]. In a typical fluorescence microscope, contrast is determined by the intensity of light collected from the specimen, the dynamic range of the signal, optical aberrations of the optical imaging system, and the number of pixels per unit area in the final image [4].

The influence of noise on the image for two closely spaced small objects is a further concept related with the aforementioned factors. It too can affect the quality of resulting images. Another important factor is the limitation on effective resolution resulting from the division of the image into a finite number of picture elements (pixels) [14,17]. All digital confocal images employ laser scanners or digital camera systems and the data are recorded and processed in terms of measurements made within discrete pixels. These measurements need to be analyzed within criteria specific to sampling theory [4].

The relationship between contrast and resolution with regard to the ability to distinguish two closely spaced sample features implies that resolution cannot be defined without including contrast, and it is this interdependency that has led to considerable ambiguity involving the term resolution and the factors that influence it in microscopy [4,18,28].

2.1 The Airy Disk and Lateral Resolution

Imaging a point-like light source in the microscope produces an electromagnetic field in the image plane whose amplitude fluctuations can be regarded as a response of the optical system to the sample. This electromagnetic field is commonly represented through the amplitude point spread function, and allows for evaluation of the optical transfer properties of the combined system components [2,11,17,19]. Eventhough variations in field amplitude are not directly observable, the visible image of the point source formed in the microscope optics and recorded by the microscope imaging system is the intensity point spread function. This describes the system response in real space. Actual samples are not point sources, but can be regarded as a superposition of an infinite number of objects having dimensions below the point spread function (PSF) in the image plane as well as in the axial direction. These are the major factors in determining the resolution of a microscope [4,11,12,13,19].

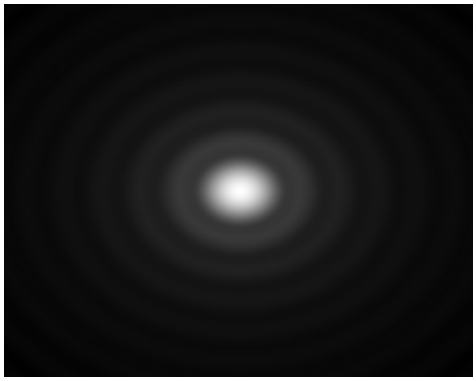

Figure 2.1 An airy disk diffraction pattern.

It is possible to experimentally measure the intensity point spread function formed in the microscope by recording the image of a sub-resolution spherical bead scanned at the focus. Because of the technically difficulty involved in the direct measurement of the intensity point spread function, such as manufacturing and placing a bead of sub-resel size, calculated point spread functions are utilized to evaluate the resolution performance, and the optical-sectioning capabilities of confocal as well as conventional widefield microscopes. Eventhough the intensity point spread function is a distribution in all three dimensions, especially when considering the relationship between resolution and contrast, it is useful only to consider the lateral components of the intensity distribution. The familiar Airy disk [4,12,24].

The intensity distribution of the point spread function in the plane of focus is described by the rotationally symmetric Airy pattern. Due to the cylindrical symmetry of microscope lenses, the two in the plane components (x and y) of the Airy pattern are equivalent. Thus, the pattern represents the lateral intensity distribution as a function of distance from the optical axis. The lateral distance is normalized by the numerical aperture of the system as well as the wavelength of light, resulting in a dimensionless quantity. Figure2.1 (airy disk and intensity function) illustrates graphicallly the formation and characteristics of the Airy disk, the related three-dimensional point spread function, and Airy patterns in a microscope. Following the the illumination by a laser in a point-like specimen region, reflection occurs in all directions, a small fraction of which is selected and focused by the optical components into an image plane where it forms an Airy disk surrounded by concentric rings of successively decreasing maximum and minimum intensity (the Airy Pattern) [4].

The Airy pattern intensity distribution is the result of Fraunhofer diffraction of light passing through a circular aperture. In an ideal optical system it exhibits a central intensity maximum and higher order maxima separated by regions of zero intensity. The distance of the zero crossings from the optical axis, being the distance which is normalized by the numerical aperture and wavelength, occur periodically (see Figure 2.1). If the intensity on the optical axis is normalized to one (highest peak), the

proportional heights of the first four higher order maxima are 1.7, 0.4, 0.2, and 0.08 percent, respectively [4].

A useful concept of resolution is based on consideration of an image formed by two pointlike objects (sample features), under the assumption that the image-forming process is independent, and that the interaction of the separate object images can be described using intensity point spread functions. The resulting image is then given by the sum of two Airy disks. The resolution of this image depend upon the separation distance between the two points. When the separation is large, the intensity change in the area between the objects is the maximum possible, going from the peak intensity (at the first point) to zero and returning to the maximum value at the center of the second point. At decreased distance in object space, the intensity distribution functions of the two points, begin to overlap in the image plane and the resulting image may appear to be that of a single larger or brighter object or feature rather than being recognizable as two objects. We define resolution, in general terms, as the minimum separation distance at which the two objects can be sufficiently distinguished. This property is related to the width of the intensity peaks (the point spread function). So that, microscope resolution is directly related to the full width at half maximum (FWHM) of the instrument's intensity point spread function in the lateral directions [4].

There is some ambiguity in use of the term resolution as the variability in defining the separation distance between features and their point spread functions that is enough to allow them to be distinguished as two objects rather than one object. Generally, minute features of interest in microscopy samples produce point images that overlap to some degree, showing two peaks separated by a gap [12,13,19,24]. The greater the depth of the gap between the peaks, the easier it is to separate, or resolve, the two objects. By specifying the depth of the intensity dip between two overlapping point spread functions, the resolution can be quantitatively and consistently described [4].

To accurately quantify the resolution, the concept of contrast is used. This is defined for two objects of equal intensity as the difference between their maximum intensity and the minimum intensity occurring in the space between them. Because the maximum intensity of the Airy disk is normalized to one, the highest achievable contrast is also one, and occurs only when the spacing between the two objects is quite large, with sufficient separation to allow for the first zero crossing to occur in their combined intensity distribution. At decreased distances, as the two point spread functions begin to overlap, the dip in intensity between the two maxima (and the contrast) is increasingly reduced. The distance at which two peak maxima are no longer distinguishable in the image plane, is referred to as the contrast cut-off distance (the contrast becomes zero). The variation of contrast with distance allows for the resolution, in terms of the separation of two points of intensity, to be defined as a function of contrast [4].

The relationship between contrast and separation distance for two point-like objects is coined as the contrast/distance function or contrast transfer function [20]. In this respect, resolution can be defined as the separation distance at which two objects are imaged with a certain contrast value. It should be noted that when zero contrast exists, the points are not resolved hence in this respect the so-called Sparrow criterion defines the resolution of an optical system as being equivalent to the contrast cut-off distance. More commonly, we specify that a greater contrast is necessary to adequately distinguish two closely spaced points visually, given by the well-known Rayleigh criterion for resolution which states that two points are resolved when the first minimum (zero crossing) of one Airy disk is aligned with the central maximum of the second Airy disk. Under ideal imaging conditions, the Rayleigh criterion separation distance corresponds to a contrast value of 26.4 percent. Although any contrast value greater than zero can be specified in defining resolution, the 26-percent contrast of the Rayleigh criterion is considered reasonable in typical microscopy applications, and is the basis for the typically used expression defining lateral resolution according to the following equation, in which the point separation (r) in the image plane is the distance between the central maximum and the first minimum in the Airy disk [4,12]:

$$r_{lateral} = 1.22\lambda/(2.NA) = 0.6\lambda/NA \quad (2.1)$$

where λ is the emitted light wavelength and NA is the numerical aperture of the objective.

In order to avoid the difficulty in attempting to separate intensity maxima in the Airy pattern, and since the resolution in the microscope is directly related to the FWHM dimensions of the microscope's pointspread function, it is common to measure this value experimentally in the image plane. This results in measurements of resolution utilizing the FWHM values of the point spread function to be somewhat smaller than those calculated employing the Rayleigh criterion. In addition, in confocal microscopy configurations, single-point illumination scanning and single-point detection are used, so that only the point objects in the shared volume of the illumination and detection point spread functions are able to be detected. Thus, the intensity point spread function in the confocal case is the product of the independent illumination intensity and detection intensity point spread functions [2]. For confocal applications, the lateral (and axial) extent of the point spread function is reduced by about 30 percent compared to that in the widefield microscope. Due to the narrower intensity point spread function, the separation of points required to achieve acceptable contrast in the confocal microscope is reduced to a distance approximated by [4]:

$$rlateral = 0.4\lambda/NA \quad (2.2)$$

Since the illumination and reflection emission wavelengths (not in the case when the reflected wavelegnth changes) are approximately the same, the confocal microscope Airy disk size is the square of the widefield microscope Airy disk. Notably, the contrast cut-off distance is reduced in the confocal arrangement, and equivalent contrast can be achieved at a shorter distance compared to the widefield illumination conventional microscopy. Whether it is confocal or conventional microscopy, the

lateral resolution is proportional to wavelength, and is inversely proportional to the objective lens numerical aperture [4]:

As noted before, lateral resolution is of primary importance when discussing resolution and contrast, however the axial extent of the microscope intensity point spread function is similarly reduced in the confocal arrangement and is also an advantage of using confocal microscopy as compared to the widefield fluorescence configuration [4,11,17,19,20,24].

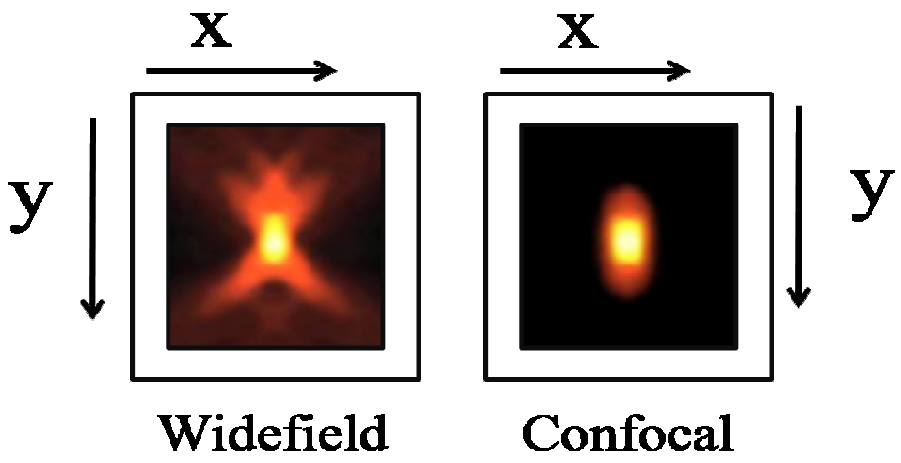

Figure 2.2. Comparison of axial (x-z) point spread functions for widefield (left) and confocal (right) microscopy.

Acceptable contrast between point-like objects lying on the optical axis occurs when they are separated by a distance between the central maximum and the first minimum of the axial point spread function component. Presented in Figure 2.2 are the axial intensity distributions for a typical widefield (Figure 2.2.(a)) and confocal (Figure 2.2(b)) microscope. Note the dramatic reduction in intensity of the "wings" in the confocal distribution as a function of distance from the central maximum. A variety of equations are presented in the literature that is based on different models for calculating axial resolution for various microscope configurations. The models most

applicable to confocal reflection imaging are similar in form to the expressions evaluating depth of field. These equations demonstrate that axial resolution is proportional to the wavelength and refractive index of the specimen medium, and inversely proportional to the square of the numerical aperture. Thus, the numerical aperture of the microscope objective has a much greater effect on axial resolution than does the emission wavelength. One such equation commonly used to describe axial resolution for the confocal configuration is given below, with η representing the index of refraction [4]:

$$raxial = 1.4\lambda\eta / NA^2 \tag{2.3}$$

Although the confocal microscope configuration exhibits only a modest improvement (30% reduction in lateral resolution) in measured axial resolution over that of the widefield microscope, the true advantage of the confocal technique is in its optical sectioning capability of thick specimens. This not only results in a dramatic improvement in effective axial resolution over conventional techniques but also allows for an accurate three-dimensional image of the object. This fine comb resolution of the confocal microscope in the axial direction results from the characteristics of the squared intensity point spread function, which has a maximum in the focal plane when evaluated as a function of depth. The equivalent integral of the intensity point spread function for the conventional widefield microscope does not produce an optical sectionining capability [4]

2.2 Point Spread Function (PSF)

2.2.1 Numeric aperture and dimensionless units

Since there are many approaches and formulas in microscopy we need some adopted terms in optics to describe optical parameters like numeric aperture which is simply represented by the symbol NA and is defined as follows [5]:

$$NA = n \sin\theta \tag{2.1}$$

Where n is the refractive index of the media, and θ is the half-angle of a cone within which light rays converge or diverge. For a lens, this angle is defined by its diameter D and focal length F [5]:

$$\sin\theta = \frac{D}{2F} = \frac{NA}{n} \tag{2.6}$$

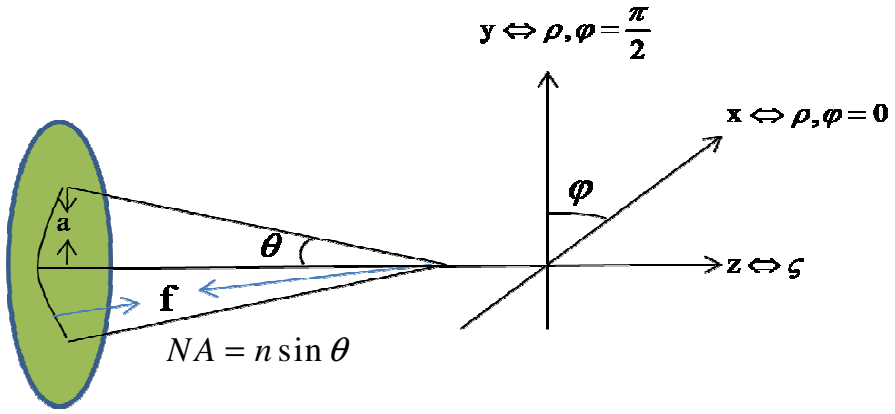

Figure 2.3 Numerical aperture (NA) the optic axis is taken along z, which is scaled to ζ *and the planes of constant* ζ *contain the scaled radius* ρ *and the azimuth* φ

It is convenient to measure distances from the axis in the object plane by the units of the light wavelength in the media $\lambda' = \lambda / n$, where λ is light wavelength in vacuum [2,4,5].

Dimensionless radius unit in this case will be written as

$$\rho = \frac{2\pi}{\lambda} NAr = \frac{2\pi n}{\lambda} r \sin\theta \tag{2.7}$$

while dimensionless distance ζ along the optical axis will be

$$\zeta = \frac{2\pi}{n\lambda} NA^2 = \frac{2\pi n}{\lambda} z \sin^2 \theta \tag{2.8}$$

Images are formed by lenses, objectives or mirrors in geometrically conjugate planes. In addition, for rays emanating from every point of the object, the Fraunhofer diffraction condition is met. For example, a parallel beam from the distant point object will converge in a lens focal plane (Fig. 2.4). Since each point in the focal plane corresponds to the point at infinity, the Fraunhofer diffraction condition is met in the focal plane. Aperture *D* which confines the beam plays the role of an obstacle for light diffraction. Such an aperture, in particular, can be the lens mount. This describes the case of the diffraction at the optical system entrance aperture [2,5].

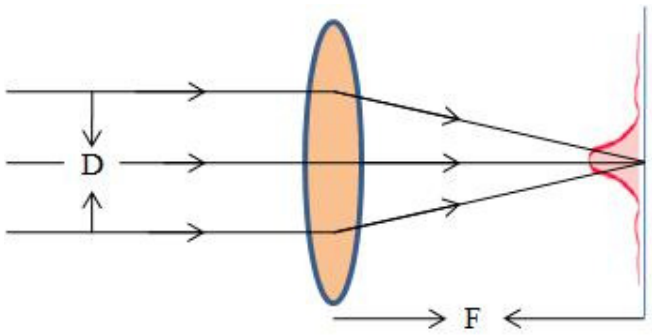

Figure 2.4 Fraunhofer diffraction in a lens focal plane.

Similarly this can be considered as the case when the point object is positioned at a finite distance from the lens and the image is formed at a distance *b* from the lens on its right-hand side. Distances *a* and *b* are related to the focal length by lens formula[5]:

$$\frac{1}{a} + \frac{1}{b} = \frac{1}{F} \tag{2.9}$$

To explain why Fraunhofer diffraction takes place here, we replace the single lens with focal length F by two closely placed lenses with focal lengths F_1 and F_2 (Fig. 2.5). The source will be positioned in the front focal point of the first lens and the image plane will coincide with the rear focal plane of the second lens. The above condition is automatically met in this case because it is equivalent to the optical power (i.e. inverse of a focal length) sum rule of two closely situated lenses. Between the two lenses the light rays travel as a parallel beam. Comparing Fig. 2.4 and 2.5 it is seen that in the second case the Fraunhofer diffraction occurs at the common lens mount and is viewed in the rear focal plane of the second lens. Fig. 2.4 corresponds to the diffraction pattern in the telescope objective, Fig.2.5 gives the light diffraction pattern in the microscope objective [5]

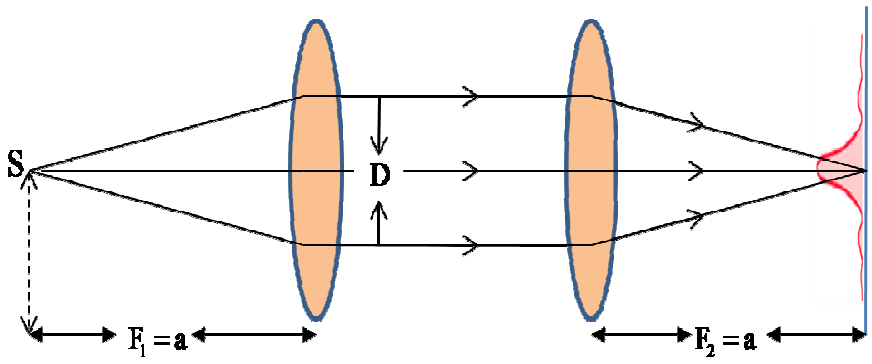

Figure 2.5 Fraunhofer diffraction in a plane geometrically conjugate with a source.

The point spread function (PSF) determines the intensity distribution in the lens focal plane due to the Fraunhofer diffraction from the entrance aperture [3]. As shown previously, exactly the same intensity distribution from a point source is formed in the conjugate plane of a thin lens [5].

PSF of the light beam limited by a circular aperture with diameter *D* for the lens having focal length *F* can be expressed in its general form as follows:

$$p(\zeta,\rho)=\left|I_0(\zeta,\rho)\right|^2+2\left|I_1(\zeta,\rho)\right|^2+\left|I_2(\zeta,\rho)\right|^2 \tag{2.10}$$

where

$$I_0(\zeta,\rho)=\int_0^{\theta} J_0(\rho\sin\alpha/\sin\theta)\sqrt{\cos\alpha}\sin\alpha(1+\cos\alpha)\exp\left(i\zeta\cos\alpha/\sin^2\theta\right)d\alpha$$

$$I_1(\zeta,\rho)=\int_0^{\theta} J_1(\rho\sin\alpha/\sin\theta)\sqrt{\cos\alpha}\sin^2\alpha\exp\left(i\zeta\cos\alpha/\sin^2\theta\right)d\alpha$$

$$I_2(\zeta,\rho)=\int_0^{\theta} J_2(\rho\sin\alpha/\sin\theta)\sqrt{\cos\alpha}\sin\alpha(1-\cos\alpha)\exp\left(i\zeta\cos\alpha/\sin^2\theta\right)d\alpha$$

where $J_k(x)$ – k-th order Bessel functions,

$$\sin\theta=\frac{D}{2F}=\frac{NA}{n} \tag{2.11}$$

Here the more general function is introduced as compared with that given before. This function $p(\zeta,\rho)$ gives the intensity distribution along radius ρ for different planes ζ. This fucntion also states that ζ [5]:

$$\int_0^{\infty} p(\zeta,\rho)\rho d\rho = const \tag{2.12}$$

which means that energy flux through every plane is constant.

In the paraxial approximation (small NA magnitudes), the light intensity distribution in the focal plane is given by:

$$p(0,\rho)\approx\left(\frac{2J_1(0,\rho)}{\rho}\right)^2 \tag{2.13}$$

where the normalization coefficient is selected so that $p(0,0)$ value in a focal point is equal to 1 [5,6].

The diffraction pattern from a circular aperture is a series of concentric rings. A central bright spot is called the Airy disk. The first bright ring maximum intensity is about 2% of the intensity in the center of the Airy disk. Distribution $p(0, p)$ is shown in Fig. 2.6

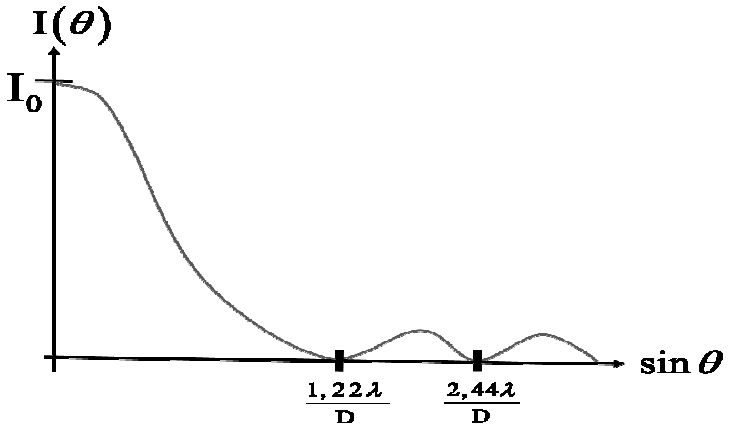

Figure 2.6 Intensity distribution of light diffracted by a circular aperture.

The Airy disk radius is:

$$\rho_{resel} = 1.22\pi \tag{2.14}$$

Or

$$r_{resel} = 0.61\frac{\lambda}{n\sin\theta} = 1.22\frac{\lambda'}{D}F \tag{2.15}$$

Where

$$\lambda' = \frac{\lambda}{n}$$

It should be noted that on the system optical axis $(\rho = 0)$: $I_1(\zeta, 0) = 0$ and $I_2(\zeta, 0) = 0$, therefore the resolution along the optical axis is determined only by contribution of $I_0(\zeta, 0)$. In the paraxial approximation (small NA magnitudes), the relative intensity distribution along the axis is given by [5,6]

$$p(\zeta, 0) \approx \left(\frac{\sin\left(\frac{\zeta}{4}\right)}{\zeta/4} \right)^2 \tag{2.16}$$

Resolution of the microscope generally means the capability to distinguish two point objects of about equal intensity. From the function of intensity distribution in a focal plane $p(0, \rho)$ it follows that the resolution is determined by overlapping of Airy disks of two point-like objects. Rayleigh proposed the criterion [10] which states that two points are resolved if a "dip" in their images intensity is 26% of the maximum intensity. Also, the separation distance between two resolved points should be more than the Airy disk radius.

To examine mathematically how much the contrast is changed when utilizing confocal microscopy, first we evaluate the PSF. Because the light in the confocal microscope passes through the objective twice, the point spreading function is given by:

$$p_{conf}(\zeta, \rho) = p(\zeta, \rho) \times p(\zeta, \rho) \tag{2.17}$$

To simplify the analysis each PSF will be qualified as a probability of a photon hitting the point with coordinates (ζ, ρ) or a photon detection from the point with coordinates (ζ, ρ); then the confocal PSF will be a product of independent probabilities. Fig. 8 shows a representation of conventional and confocal PSF [5].

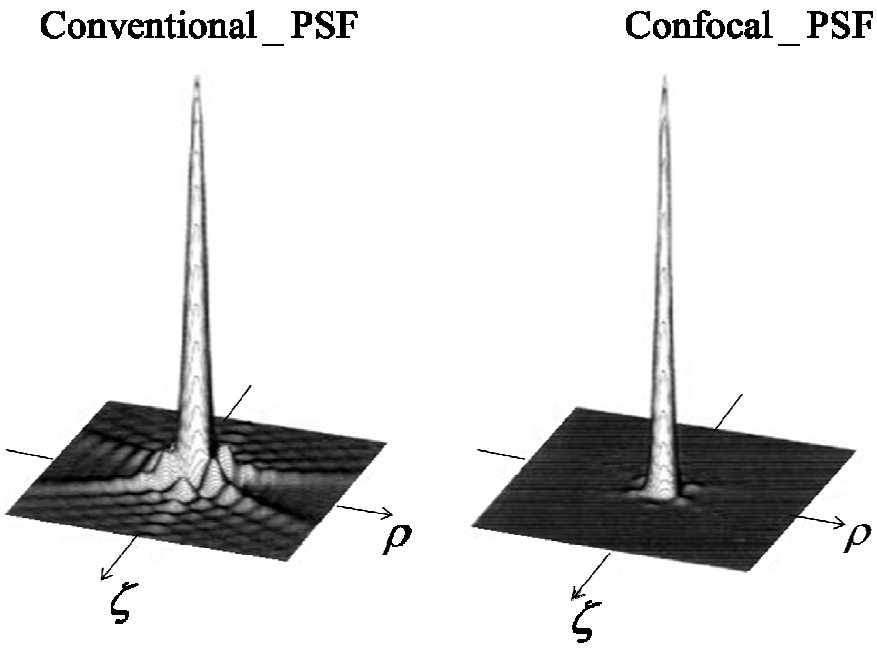

Figure 2.7 Confocal PSF $p_{conf}(\zeta,\rho) = p(\zeta,\rho) \times p(\zeta,\rho)$ *is shown on the right, conventional PSF* $p(\zeta,\rho)$ *– on the left, addopted from [5].*

If we use the Rayleigh criterion for the resolution (26% dip of the maximum intensity), the result is a slight increase in resolution for the confocal microscope compared to the conventional microscope:

$$r_{conf} = 0.44\frac{\lambda}{n\sin\theta} = 0.88\frac{\lambda'}{D}F \tag{2.18}$$

The conventional optical microscope resolution is given by

$$r_{resel} = 0.61\frac{\lambda}{n\sin\theta} = 1.22\frac{\lambda'}{D}F \tag{2.19}$$

Where : $\lambda' = \lambda/n$

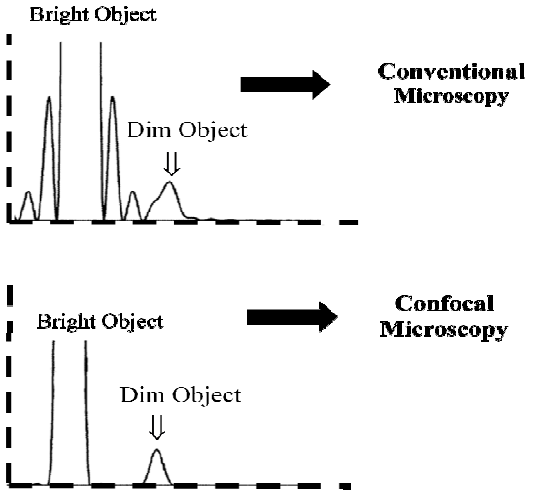

Figure 2.8. Intensity profiles for conventional (top picture) and confocal (bottom picture) microscopes. Intensity maximum of the dim object is 200 times less than that of the bright one.

The major advantage of a confocal microscope is a larger increase in the contrast rather than resolution improvement in accordance with the Rayleigh criterion. In particular, the relation of the first ring maximum amplitude to the amplitude in the center is 2% in case of conventional PSF in the focal plane while in the case of a confocal microscope this relation is 0.04%. The practical importance of this factor is illustrated in Fig. 2.8 From the top part of the picture it can be seen that a dim object can not be as well detected in a conventional microscope eventhough the separation distance between objects exceeds that of the Rayleigh criterion. In a confocal microscope (bottom part of Fig. 2.8) this object can be well observed [5].

The intensity distribution along the optical axis in a confocal microscope is given by the following expression:

$$p(\zeta,0) \approx \left(\frac{\sin\left(\frac{\zeta}{4}\right)}{\zeta/4} \right)^2 \tag{2.20}$$

Then, using the Rayleigh criterion [10] the resolution in the direction along the optical axis is given by:

$$\Delta z_{conf} = 1.5\frac{\lambda}{n\sin^2\theta} = 1.5\frac{n\lambda}{NA^2} = 6\lambda'\left(\frac{F}{D}\right)^2 \tag{2.21}$$

2.2.2 The effect of an aperture in a focal plane

It is important to distinguish this resolution and depth of focus for a conventional microscope [1-3]. In these cases, the depth of focus is hundreds times more than the resolution along the optical axi [5,6]

One parameter which was not taken into consideration in the above analysis, is the size of an aperture in a focal plane of illuminating and collecting lenses. Nwe calculated the PSFs for conventional and confocal microscopes under the assumption that the illuminating source was point-like. Therefore the PSF we obtained described properties of an objective lens, while the aperture image in the object plane determined the area whose light is detected by the photodetector. Lowering the aperture size decreases the amount of the passing light, increases noise level and, finally, can reduce all the aforementioned advantages in the contrast. Thus, it is important to choose an aperture of optimal size and the resulting compromise needs to be addressed [5]

The use of an aperture with a size which is less than that of the Airy disk is at the limit of the onset of intensity loss and does not affect the resolution. If aperture size is that of the Airy disk, the objective lens resolution is maximized. The best compromise, however, is to choose an aperture size which is 3-5 times more than that of the Airy disk. This size is referred to as the actual image size in the object plane, hence the actual aperture size also depends on the lens magnification [5].

In order to consider mathematically the presence of an aperture and to obtain a new function of intensity distribution one needs to convolve the aperture with the PSF

$$P(\zeta,0) = p \otimes S = \int p(\rho - \rho_s, \zeta) S(\rho_s, \varphi_s)\, \rho_s d\varphi_s d\rho_s \tag{2.22}$$

and for a confocal microscope this mean that we needs to multiply the obtained function $P(\rho,\zeta)$ by $p(\rho,\zeta)$. The resulting intensity distribution in case of the aperture size of 5 Airy disks is shown in Fig. 2.9 [5].

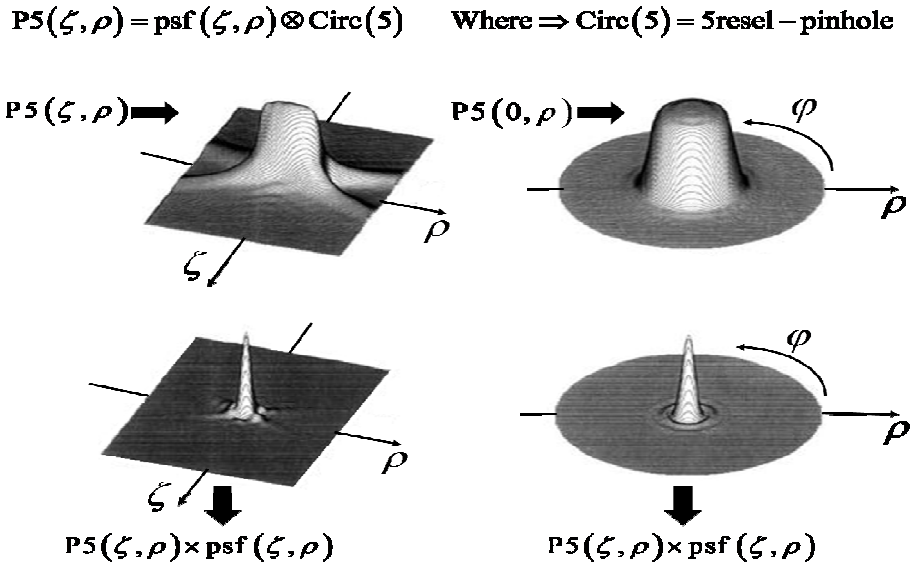

Figure 2.9 Point spreading functions for conventional microscope with an aperture size of 5 Airy disks (top pictures) and for confocal microscope (bottom pictures), Addopted from [5].

CHAPTER 3

EXPERIMENT AND RESULTS

In CSLM, confocal imaging can be achieved in two ways: first one is leaving the optics fixed and moving the object while the second one is to move the laser beams rather than the object itself. Moving the object is the simplest way and has two major advantages: all the lenses work on axis, and the field of view is not constrained by the optics. Lenses can easily be diffraction limited for the single on-axis focus. It is easy to guess that the very first versions of confocal microscopes were stage scanners. On the other hand, for reasons of speed in image acquisition it makes sense to move the laser beams rather than the object. This way we are able to observe a wider field of view on the object with roughly the same resolution. Most developed confocal microscopes use this approach, with the beam scanners most typically small mirrors mounted on galvanometer actions.

There is also another way to move the laser beam on the object and that is by the help of an optical fiber. In the fiber system the main part of the fiber is used to transmit the beam while the outer fibers are used to collect the image. Afterwards galvo-mirrors can be utilized to scan each fiber. In the further steps in our project we are going to use the advantage of fibers to move laser beam on metal surfaces but for now we demonstrated the fundamentals of confocal imaging with a stage scanner type of confocal imaging system.

3.1 Experiment

The following sections explain how to build a stage scanning confocal imager and apply it towards imaging various metal surfaces. The experiment is analyzed by focusing on lateral (x, y) and axial (z) resolution parameters and how these

parameters are affected by the focal spot size as well as the size of the iris on the detector. In this experiment speed was not a main concern hence the stage scanning used servo motors which were already in hand. While these motors allowed us to perform the imaging their speed limited us in achieving true video rate imaging.

3.1.1. System Construction

We designed an imaging system based on confocal techniques in the laser laboratories in the Physics department at Middle East Technical University (METU). We did not have the ideal equipments yet for well-qualified (video-rate) imaging but we did have sufficient equipment to analyze various metal surfaces based on confocal principles. During the discussion we will discuss which parts had what kind of problems due to lack of ideal equipments and tools.

The laser source was an 808-nm fiber-coupled (multimode fiber) diode laser. We measured the output power before and after the fiber coupling. Our power measurements showed it produces roughly 780mW power just after the beam leaves the fiber.

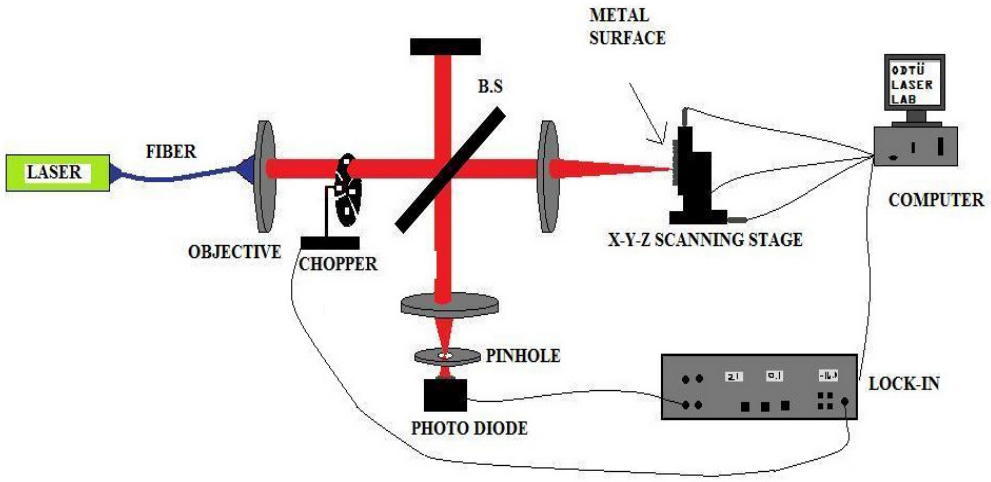

Figure 3.1 Our CSLM schematic diagram

Laser beam diverged rapidly after leaving the roughly 100μm diameter core MM-fiber so we attached a collimating lens that allowed the beam to propagate with roughly a 5mm diameter with little or no divergence across the set-up. Our detector was a Silicon PIN photodiode, which although is very sensitive may not have been able to resolve the minute differences in intensity typical to a confocal imager. Typically in CSLM systems the photo-detector is either a Photomultiplier Tube (PMT) or Avalanche Photo-detector (APD) depending on the illumination source wavelength. Due to the fact that we were using a regular Si-PIN photodiode we did not want to risk measuring too much noise so we opted for phase sensitive detection of the returned signal using a lock-in amplifier (SR530 Dual Phase lock-in amplifier). Since the beam was roughly 5mm in diameter we were forced to amplitude modulate the beam with a large throughput mechanical chopping blade. The mechanical chopping (SR 540, 5- spoke blade) was done at 400 Hz (maximum for the 5-spoke blade with the large holes). The complete system is illustrated in figure 3.1.

As can be seen the beam passes the mechanical chopper where it loses roughly half its power and then propagates across a 50:50 beam splitter onto a 2.5x focusing planar (infinity corrected) objective onto a metal surface attached to an XYZ-stage scanner. The scanner stage was driven by three separate DC servo motors. The reflected beam off the surface was sent back through the objective onto the beam splitter and reflected onto a pinhole and subsequently a Si-PIN photo-detector. At this point a personal computer (PC) was used to both control the stage and the lock-in amplifier and plot the data. While this is not a true confocal imager in the sense that the focus to the laser beam from the 2.5x objective is not equal to the distance to the photo-detector, it is similar in the fact that we used another lens (similar to the objective used to collimate the laser beam) on the detector arm to foreshorten the distance the beam has to travel onto the photo-detector. In the future we will expand the laser beam to simulate it as a point source and will not use the objective to collimate the beam coming from the laser and the lens to focus the detected beam onto the Si-PIN photo-detector.

3.1.2. Measurements

The laser source we used produces nearly 1000mw of average output power but the beam passes through many optical instruments like; a fiber, chopper, lenses and a beam splitter so the intensity of the beam decreases until it arrives at the photo-detector. We made power measurements along the beam and the power measured after the beam collimating lens was 780mW. At the focus of the 2.5x objective the power was measured to be 228mW and after the focusing lens and pinhole (100 micron) it was measured to be roughly 16mW.

Initially, after we completed the experimental setup and checked the power of the laser source, we performed a manual measurement by manually moving the XYZ-stage to see the fluctuations on the received signal on the lock-in amplifier (SR 530 Dual-phase lock-in amplifier). We moved the stage through x, y and z axes on various metal surfaces such as damaged metal slabs and various metal coins. We observed that the voltage (received signal which lock-in measures) varies by moving the stage as we expected. This means that the surface variations translate into voltage variations. These variations in voltage could then be imaged by computer programs while at the same time the stage could be controlled by a computer program as well. The control of the stage was done through DC servo motors, which required us to use a driver which could be controlled by a PC. This automated PC control allowed us to obtain many more data values than we could have if done manually and at higher speeds. This allowed us to obtain accurate images of the surfaces we investigated.

The stage (Thorlabs 25mm travel metric stage with 3 ZB625 DC servo motors attached, each with max 25mm travel, driven by API Technologies DXI-PCI100 8-axis stage controller PCI card and each axis was equipped with a MT-110 servo motor driver) can be moved in 3-directions by a computer program, namely a National Instruments Labview7.1 based computer program which we wrote specifically for this experiment. The program had to not only control the XYZ-stage through the controller card but also the lock-in amplifier through GPIB connection. The computer program had to accommodate the experimental needs of the measurements. For example, we set the lock-in time constant to 300ms because this

time constant has to be much larger than the chopping time. For our experiment the chopping time was:

$$\frac{1}{400Hz} = 0.0025s = 2,5ms \tag{3.1}$$

This meant that the program had to be relatively fast so that the execution time would not interrupt the data acquisition times. The detection of the reflected beam intensity was done with a silicon PIN photodiode (Electro-Optics Technology ET2000, rise time 200ps and responsivity at 830 nm is 0,4mA/W) for detection.

3.1.3. Computer Program

Confocal microscopy is based on focusing the light on to one point on a plane and imaging that one point at one plane at a time. Moving the z axis additionally to the x and y axes let us gain the 3D image of the scanned surface. In the beginning, we fixed the z axis on the focus of the objective, the point where we received the most reflected signal. Since our z axis is fixed our stage moves through the x and y axis for fixed z positions and in doing so we were able to scan various metal surfaces within the restricted 25mm range of the servo motors.

Our scanning procedure stands on very simple idea. One axis moves continuously while the other axis, which is called step axis, is moved in discreet steps. After the continuous axis arrives at a desired point the step axis takes a step and then the continuous axis starts scanning in reverse from the new value of the step axis. This procedure then is reversed once again. This scanning method is shown schematically in figure 3.2.

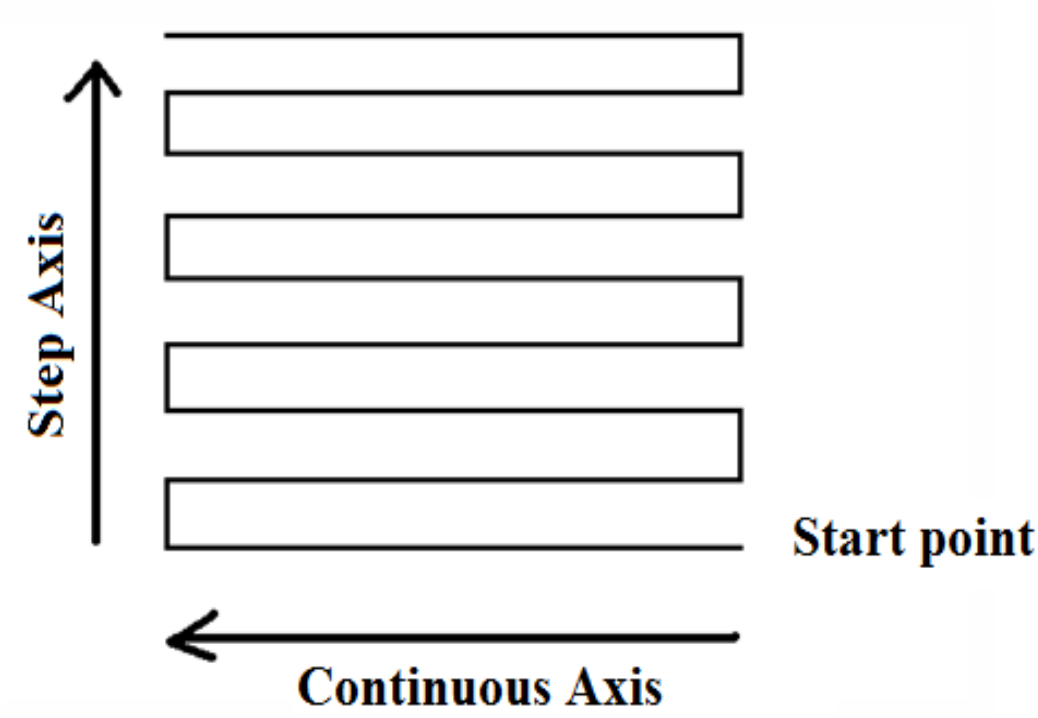

Figure 3.2 schematic diagram of scanning procedure

Since the DC servo motors are open-loop, i.e. there is no feedback mechanism to inform the computer of where the motor is the DC servo motors had to be initialized to a certain position before scanning. This allowed us to define an absolute zero point for each individual motor. The motions or trajectories in the program were performed with respect to this absolute position. The initialization procedure works like Each motor is moved to the end of their travel range and then the motor is adjusted to a position slightly above this maximum position for each axis. This was our absolute zero. In doing so, we were able to keep at least 24-25mm travel range for each axis. This part of the computer program was written by LabView7.1 and the screen image of this program is shown below.

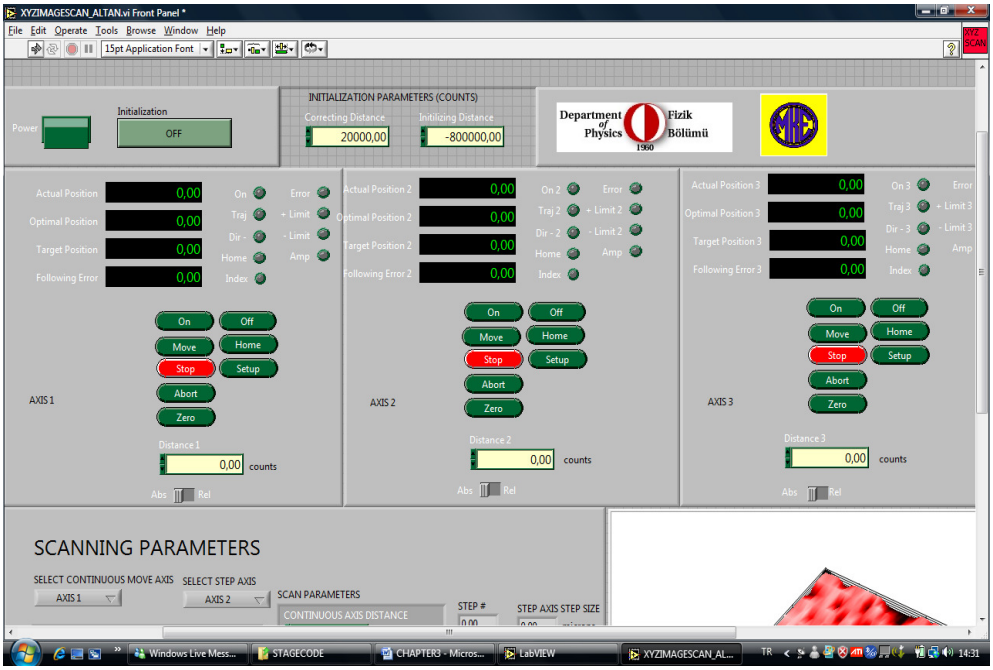

Figure 3.3. Initialization and axis control part of of the X-Y-Z image scan program.

After initialization we need to be able to adjust each axis with respect to absolute zero. This program allows us to move each axis in the units of the DC motors which our counts. Our trial measurements, basically these were measurements done to calibrate each axis to a length in mm, show that each axis moves roughly 25mm for 600000 counts. The smallest motion that each axis can perform was roughly 12 counts. It is important to note that for DC servo motors without feedback these measurements will change for various torques about the axes (i.e. weight of object on stage).

To obtain the images as outlined in the scanning procedure in fig. 3.2, there is an important point in the scanning procedure; the scanning code has to be able to continuously scan in x, step in y and reverse the order for each y-step. Also the user can continuously scan in y and step in x. For the purpose of describing the functioning principle behind the computer program the procedure below explains the motion for x-continuous and y-step.

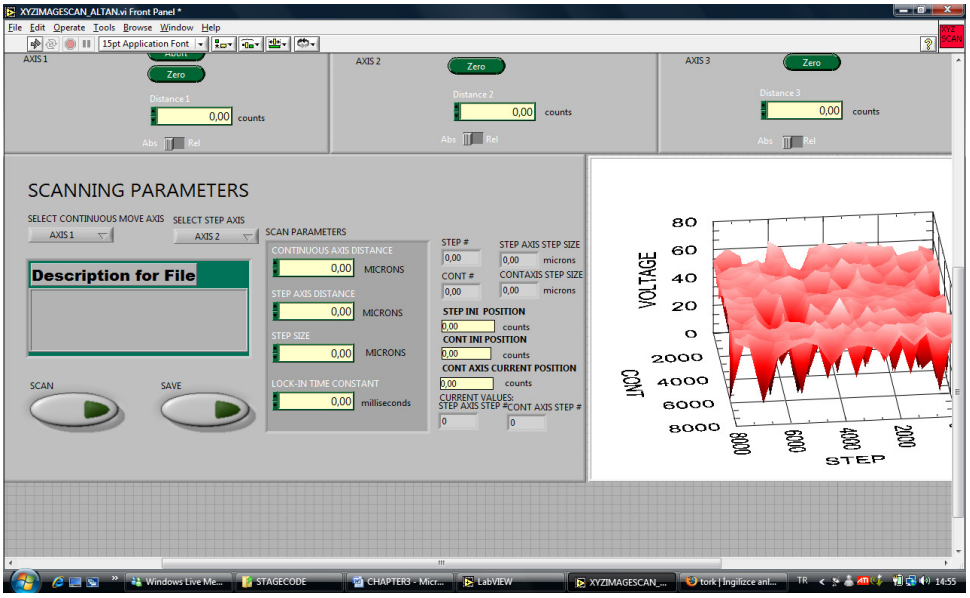

Figure 3.4. Scanning parameters for obtaining images part of the program

Finally, the program works by taking continuous voltage measurements as the x- axis moves continuously. This determines our x- axis resolution which is ultimately limited by our system resolution which is dependent on the objective. When the illumination and detection employ the same objective and the same wavelength, the lateral resolution can be expressed by the full width at half maximum (FWHM) of the confocal lateral point-spread function:

$$r_{xy} = \frac{0.61\lambda}{\sqrt{2}NA} \tag{3.2}$$

where r_{xy} is the lateral resolution, λ is the incident wavelength, and NA is the numerical aperture of the objective [29]. In our setup NA 0.07 objective was used. The lateral resolution of our system is

$$r_{xy} = 4.98.10^{-6} m \tag{3.3}$$

The pinhole size is related to the size of the Airy disk projected onto the pinhole plane for the optimal resolution and intensity. The focal spot diameter on the pinhole can be calculated from:

$$d_p = 2\frac{f_{dobj}}{f_{ep}} M_{obj} \frac{0.61\lambda}{NA_{obj}} \tag{3.4}$$

In our set up f_{dobj} = detection lens = 35 mm, $f_{ep} \approx f_{obj}$ =43.1 mm and M=2.5x, so the focal spot diameter for our setup is :

$$d_p = 28.59.10^{-6} m \tag{3.5}$$

The ideal axial resolution can be evaluated by the FWHM of the axial point-spread function:

$$r_z = \frac{2n\lambda}{\sqrt{2}NA_{obj}} \tag{3.6}$$

where n is the refractive index of the medium. In our setup, NA=0.07 for the objective, with a medium refractive index of 1.5 and an illumination wavelength of 808 nm, then resolution is:

$$r_z = 24.49.10^{-6} m \tag{3.7}$$

These parameters are the theoretical expected parameters and any deviations in the experimental results will be discussed later on in the discussion part of this chapter. As we executed the program we saw that the open-loop servo motor performance changed day to day depending on how well the ball screw inside the motor was greased or how well the motors responded to various torques about their translation axis. In addition to these effects initial investigations allowed us to correct for errors in our control code. These are discussed in the next section.

3.1.4. Results

Initially we performed measurements on simple durfaces such as a circular ring on top of a metal surface. These allowed us to refine our initial code. Also images shown using LabView was also generated using MATLAB code. The code used to generate the images in MATLAB is attached in Appendix A.

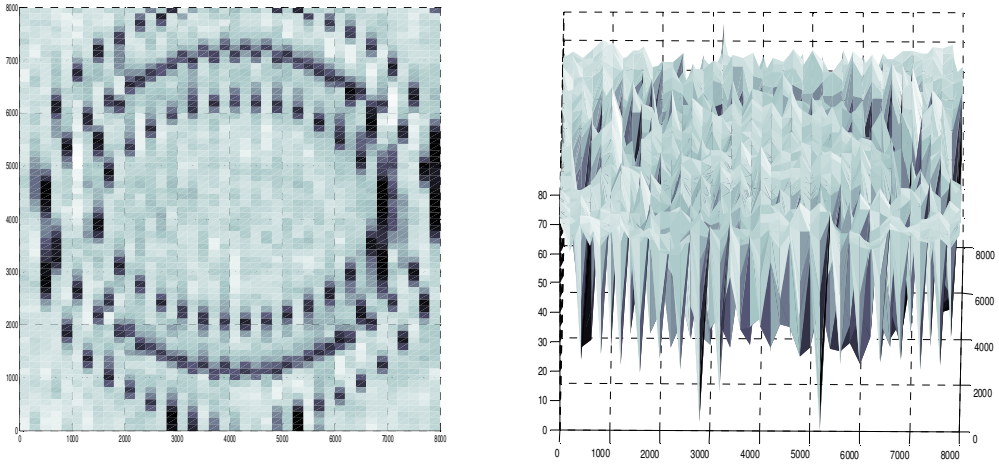

A **B**

Figure 3.5 Image of the circle on a coin with error in the code (A), 3-D image (B)

In Fig 3.5, what is shown is supposed to be an image of a circle but since there was an error in the code we see two nested circles. There was a problem in how the code formed and recorded the matrix array of voltage values. When the computer code was recording values as the continuous axis revered its direction it did not taken into account the direction reversal. We solved the problem by adding a reverse 1D array procedure to the Labview code. The images taken after the correction are shown below**:**

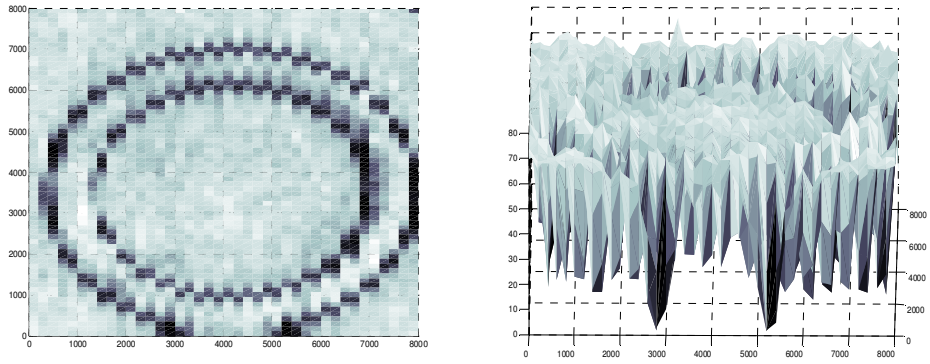

C **D**

Figure 3.6 Image of the circle on a coin with the corrected code (C , 3-D image (D)

After we fixed the errors associated with the code we examined more complicated surfaces. This tested our systems continuous axis and step axis resolution.

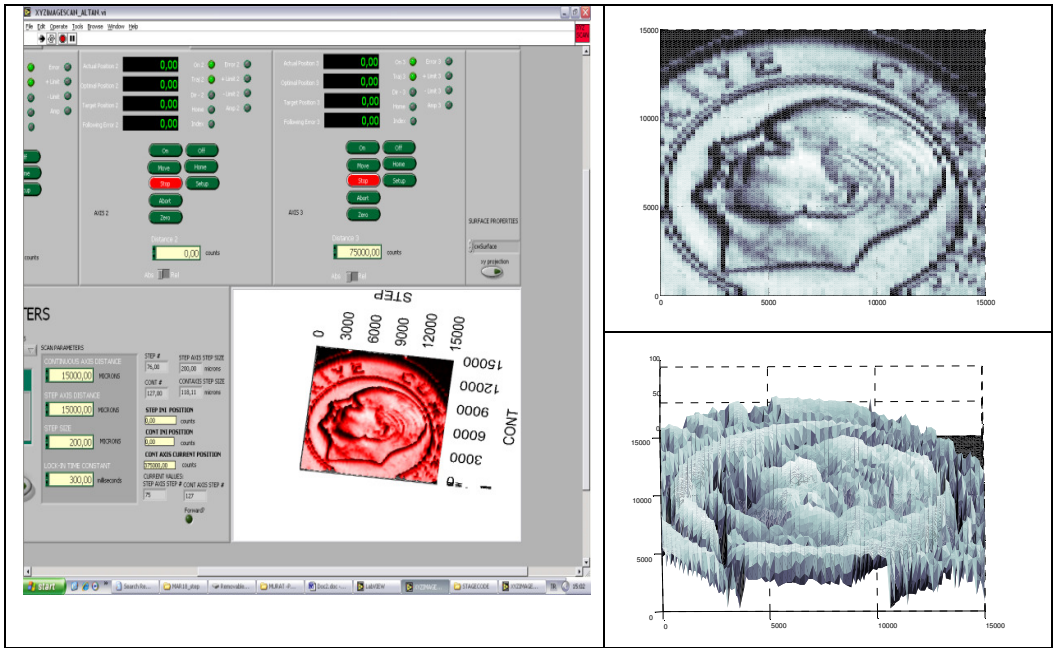

E **F**

Figure 3.7 15x15 mm image of Ataturk picture on Turkish Kuruş (C), Matlab graphs of the same Picture (D)

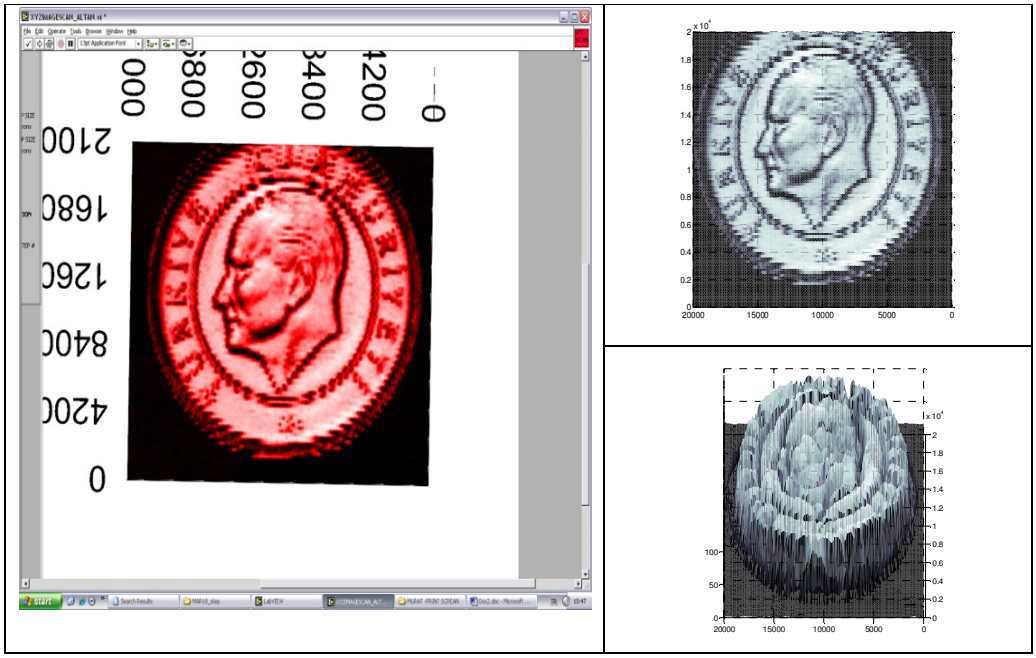

G **H**

Figure 3.8 20x20 mm image of Ataturk picture on Turkish Kuruş (E), Matlab graphs of the same images in figure (F)

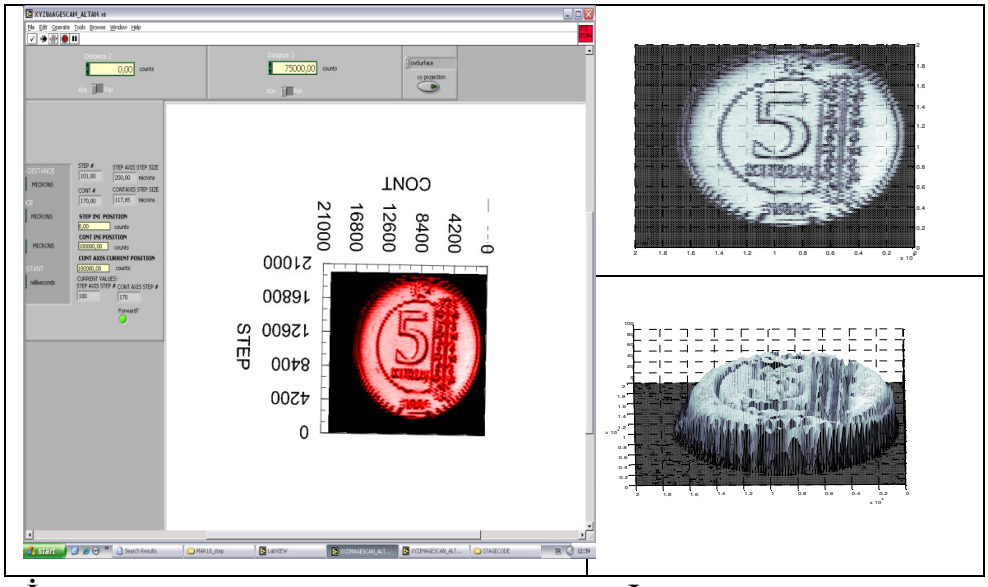

İ **J**

Figure 3.9 20x20 mm image of 5 Turkish Kuruş (G), Matlab graphs of the same image (H)

These images not only show the fine lateral resolution in the xy-directions but also the axial resolution as seen by the side view profiles of the data. Clearly, the protruding surfaces results in larger signals while the surfaces behind result in a less signal. The edges of each protrusion or indentation result in a near zero signal. This is due to the scattering of the laser intensity at that point.

3.2. Discussion

We have performed many measurements with the help of DC servo motors and our code. In our very first measurements, which were taken manually, we used a special coin and performed the measurement on the circular protrusion of that coin. We found the maximum voltage value on the coin surface by moving the z axis manually and we noted the corresponding z axis reading. Then we focused the laser beam on the circular ring prominent with respect to the coin surface and moved the z axis until we found the maximum voltage value on the lock in. The difference between the two readings was $27\,\mu m$ and the measurement result of circle height with the Vernier caliper was $28\,\mu m$. This was an important measurement because it proved to us that our system was working compatibly to confocal principles.

In confocal imaging the pinhole has major significance because optical sectioning is possible with a pinhole. It reflects the external light which comes from out of focus thus we see much sharper images. A pinhole smaller than one resel (half the separation of the first dark fringes of airy disk) does not improve resolution, it just loses light. A pinhole 1 resel across allows full use of the objective lens' resolution, but does not actually change the resolution. A pinhole three resels across seems to be a good compromise (reference). We used 100 μ m pinhole and the resel for our setup was:

$$\rho_{resel} = \frac{0.61\lambda}{NA} = 7,04\mu m \tag{3.8}$$

The pinhole we used is nearly 14 times bigger than the resel, so the pinhole we used is much bigger than we had desired. The axial resolution is given by:

$$\Delta z_{axresel} = \frac{1.5n\lambda}{NA^2_{obj}} \tag{3.9}$$

To analyze the axial resolution for a coin sample we took images of a certain part of a Turkish 25 Kuruş coin piece for different z axis values. The focus of the objective was measured to be at 72000 counts away from the initial position for the z-axis servo motor. We took a few images between 57000-92000 counts and three of them is shown in figure 3.10. The difference = 35000 counts corresponds to roughly 1,4 mm.

Figure 3.10 Images of the same part of 25 Turkish Kuruş for different z axis. Fist image was taken when z axis is on 52000 counts, middle image was taken on focus point which is 72000 counts and the last image was taken when z axis is on 72000 counts (A), matlab graphs of the same images (B)

1.4 mm is a big distance for a confocal imaging system and we were expecting major changes in the images taken for different z axis values. Since the pinhole is not as good as we desired, laser beam passed through the pinhole easily and it didn't reflect

the beam which came from out of focus. This meant that the images taken at different z-axis positions were almost all the same.

For our previous manual measurement of the circular ring on the special coin surface we had measured precisely the protrusion on the surface. We associate this to the fact that the change in the voltage when we moved the special coin in the z-direction was only 85% of the value at the maximum position. This means that even though we were moving the 25 Kuruş piece in the z-section much further the intensity changes on the order of 70-80%of the maximum value attained at 72000 counts was not enough to see the z-axis resolution. And this is due entirely to the fact that the only pinhole we had during the measurements had a size of roughly 100 microns.

There is also another significant problem involving the stages. Since we are working in micron scale it is very important to achieve scanning correctly. The servo motors have some handicaps for scanning. First one is they don't move fast enough and it makes our scanning really slow. The second one is the error in position of the servo motor is really high with respect to our scanning parameters, so it causes shifts during scanning and data collecting. These effects result in a blur of the image and these can be corrected with better stages.

CONCLUSIONS

The goal for today's technologies is to achieve better and more affordable imaging systems with higher resolution. Although microscopes have their advantages and disadvantages in the analysis of many samples available to the researcher, a laser based confocal imaging system may be better in terms of cost and contrast. As a laser based system CSLM (confocal Scanning Laser Microscopy) is a useful tool for acquiring qualitative images of scanned objects and surfaces. Furthermore it is possible to create 3-D images with the help of appropriate computer programs, a task not available to 2D wide field microscopes. CSLM offers a good deal of flexibility as a research tool, for example they can be easily modified and provide the researcher the opportunity to experiment with a variety of different configurations. Short scan time, higher axial or lateral resolution (depending on the point spread function), real-time imaging capability, cost, system size are some of the main attributes of the system.

These attributes were all examined in the application of this thesis. The goal was to examine how these parameters affect the image. The image quality is defined by achieving a good contrast and resolution. These two parameters are affected by all of the aforementioned attributes. Resolution in a CSLM system can be controlled by changing some parameters in overall design of the system. Theoretically we know the factors that affect axial and lateral resolutions. Those that affect the axial resolution are the objective numerical aperture (NA) and pinhole diameter. Increasing the NA and/or decreasing the diameter of the pinhole will increase the *z*-resolution or the axial resolution. Those that affect the lateral resolution are determined by the point spread function (PSF) at the object plane (after the objective). It is important to note that the light collected at the pinhole can also be describes as a PSF, and the restrictions on the pinhole size will allow for better axial resolution.

The point spread function (PSF) describes the response of an imaging system to a point source or point object. A more general term for the PSF is a system's impulse response, the PSF being the impulse response of a focused optical system. The PSF in many contexts can be thought of as the extended blob in an image that represents an unresolved object. In functional terms it is the spatial domain version of the modulation transfer function. It is a useful concept in Fourier optics, astronomical imaging, electron microscopy and other imaging techniques such as 3D microscopy (like in Confocal laser scanning microscopy) and fluorescence microscopy. The degree of spreading (blurring) of the point object is a measure for the quality of an imaging system.

The spatial extent of the PSF differs for coherent and incoherent light sources. One can achieve a tighter focus with the beam from a laser than an incoherent source such as a white light lamp. Due to this tighter focusing the lateral resolution of a laser based illumination scheme is better than an incoherent scheme. The PSF is also affected by the shape of the beam whether it has a Gaussian intensity distribution or other (i.e. Flat top, etc.). The PSF also exists at the pinhole for a confocal imaging system. The pinhole restricts the PSF coming from the object plane. The convolution of the PSF at the object plane with the PSF at the detector plane (at the pinhole) will tell us the degree to which we can clearly image the object. The diameter of the pinhole is selected based on this calculation. Too large of a pinhole will allow the entire PSF to be imaged on the detector, and while lateral resolution would not be affected axial resolution will. Typically, a pinhole diameter with at least 3 times the size of the lateral resolution is chosen to image the object effectively laterally while restricting the resolution axially [2].

The PSF and the lateral and axial resolution can all affect the quality of the image. One aspect of CLSM systems is that since we use a pinhole the image can be acquired with a point-like detector. This is sometimes necessary since the pinhole may restrict the incoming light onto the detector to the extent that you need very sensitive detection. A CCD camera may allow for fast imaging but in terms of signal

gain per incoming photon, a photomultiplier tube or an avalanche photo diode is preferred in most CLSM systems. This not only increases the overall sensitivity but also decreases the overall cost of the system dramatically. The disadvantage is that the image acquisition speed suffers since the image has to be built up point to point. For this reason either the object or the beam has to be scanned for the image acquisition. Since we are able to achieve scanning by two ways; moving the beam on the investigated surface or moving the surface under a fixed beam, different scanning architectures are designed. Each has its advantages and disadvantages and both are customizable systems. The beam can be moved over the surface by the use of galvanometer action mirrors or selective illumination methods such as patterned spinning disks. The latter serves as a pinhole at the same time, allowing for axial resolution. Some scanners are: Petran's tandem scanner, the Nipkow disc, Kino's single-sided disc, video rate confocal laser microscopes, multisided mirrors, Koester's three-sided slit scanner, Brakenhof's two–sided slit scanner [1,2]. In this thesis the scanning was done by moving the object around the focus of the illumination.

The method of image acquisition we developed in the confocal laser scanning microscope we constructed here in METU (Middle East Technical University) Laser Laboratory is based on scanning the object placed on a xyz-stage. The system was developed to demonstrate the fundamentals of confocal imaging that uses a stage scanner and point detection.

The laser source which had a fiber coupled output was collimated with a lens whose conjugate was placed at the detector plane to approximate the confocal imaging system principle of image acquisition. The system's properties such as axial and lateral resolutions were defined in chapter 3. The lateral resolution allowed us to investigate a variety of metal surfaces. We specifically chose metals whose surface features were at or near the lateral limit. The axial resolution determined by the pinhole size was not quantified well due to the large extent of our pinhole. Our pinhole was more than 10 times larger than the lateral resolution. While this allowed

us to obtain clear images, we could not distinguish clearly the images in the axial direction for different planes. The images were acquired using LabView based codes we wrote to control the xyz stage and the detection electronics. The images were compiled on a PC and also analyzed using code written in Matlab software. These results were presented in chapter 3. Since we were examining metal surfaces which have a large reflectivity in the visible range which we performed our measurements at a silicon (Si) PIN photodiode was sufficient for the detection. The analog signal from the photodiode was measured using phase sensitive techniques and digitized through a data acquisition card.

While there are hardware limits on the system resolution which can be analyzed through the images, an important factor was the software limits imposed by the speed of the data acquisition. This factor which can contribute to decreased sample resolution is the optical sectioning rate. This rate is a measure of the spacing between successive optical sections (step-size) and not the actual "thickness" of the optical section itself. Thus the lateral resolution was actually limited by the step size along the lateral x and y directions. Since our axial resolution was not limited by the size of our pinhole our images in the axial direction did not show any change in quality as much as we would have expected (see Chapter 3 discussion part). However, if axial resolution was near the limit we stated, it would have also been affected by optical sectioning done by the control software. To maximize the information in the images obtained, ideally we would like to acquire the images at the same resolution as the axial resolution, an optical section series (contiguous optical sections through *z*) will contain all possible sample information. Decreasing the number of optical sections through a given axial dimension may yield similar results, and will decrease the total scanning time and needs to be better investigated in the future once the axial resolution can be achieved with a better sized pinhole.

This is why scan time is also another important factor in system design. In biological application or imaging of micro objects resolution is the determinant factor of system design but when we deal with bigger objects and surfaces scan time becomes an even

more important factor. Our experimental setup was designed as a stage scanner type of confocal imaging system, so the scan time is restricted by the speed of the servo motors and it was the main reason why we couldn't take measurements in the theoretical limits of resolutions as well as at near real time speeds (30 frames per second). Since we were using DC servo motors the lateral axes in the image were separated into a stepped axis and a scanned axis. This was we were able to increase resolution along one lateral direction while increasing speed of image acquisition. Basically, it is faster to acquire data while moving then to move stop acqiore and then move again. Thus our images had a continuous axis which had a higer resolution than the step axis, since the step axis distance was ultimately controlled by our input. This resulted in non-square matrix images, which could add distortion to the image when plotted using a computer based program such as Matlab on a PC monitor. Thus it would be better to obtain square images however that would mean an increase in the image acquisition time. Typical scanning times in our system were on the order of a few hours for a 25mm x 25mm scanning plane. Since we cannot control the speed of servo motors; even decreasing continuous and step axial resolutions to half make the scan time increase excessively.

In addition to the scan time, as a limiting factor, another important limitation was that we were not able to truly realize the full advantage of the CSLM system since were did not achieve sufficient axial resolution. The pinhole has very important role in confocal microscopy since and optical sectioning in the axial direction is possible with a suitable pinhole. We have seen also experimentally it should be chosen compatible with theoretical calculation of pinhole; otherwise it is not possible to observe optical sectioning for z direction. During the discussion in Chapter 3 we note that compared to the theoretical results, the experimental results lack due to the fact that the pinhole we used was not an ideal pinhole. We hope to solve the pinhole issue by using a better pinhole selected accordingly to the lateral resolution we expect to achieve as mentioned before. In future designs of the system we hope to solve the problem of the pinhole in a simple and efficient way by the help of fiber bundle before the detector. Another issue we would like to investigate is to illuminate the

object without conditioning (collimating) the laser beam to achieve a true confocal imaging system. We will expand the laser beam to simulate it as a point source and will not use a lens to collimate the beam coming from the laser nor will we use the lens to focus the detected beam onto the Si-PIN photo-detector. Using a fiber bundle will allow each fiber in the bundle to act like a pinhole.

To conclude, in this thesis, we explain the fundamentals of an optical system, which is based on confocal imaging principles. Also we constructed a confocal laser based scanning microscopy system in our laboratory (METU Laser Laboratory) and showed the effects of the important features in CSLM systems. We saw that our measurements were clearly effected by the choice of the size of the pinhole in the axial direction of our images. However, results of this work such as the lateral resolution was enough to prove high resolution imaging is possible without the use of CCD technology. The foundations which we established for the overall system design will allow us to better design imaging systems for specific tasks. Since all imaging instruments have physical limitations on the maximum resolution and signal obtainable, applying correct software can help to overcome these hardware limitations, and maximize the imaging potential from your instrument. By setting up the instrument optimally for your particular experiment, and correctly processing the imagery, you can acquire images with a high resolution.

REFERENCES

[1] Timothy R. Corle and Gordon S. Kino Confocal Scanning Optical Microscopy and Related Imaging Systems, page 33-35, New York, NY : Springer, c2006.

[2] Timothy R. Corle and Gordon S. Kino Confocal Scanning Optical Microscopy and Related Imaging Systems, page 69-71, New York, NY : Springer, c2006

[3] Confocal Microscopy ,Denis Semwogerere Eric R. Weeks ,Emory University, Atlanta, Georgia, U.S.A.

[4] http://www.olympusfluoview.com/theory/resolutionintro.html, 15.04.2009

[5] Robert H. Webb, "Confocal optical microscopy" Rep. Prog. Phys. 59 (1996) 427-471.

[6] Richards B. and Wolf E., "Electromagnetic diffraction in optical systems II. Structure of the image field in an aplanatic system" Proc. R. Soc. A 253 (1959) 358-379.

[7] Confocal Microscopy Opens the Door to 3-Dimensional Analysis of Cells, R.E. Rowland and E.M. Nickless Institute of MolecularBio Sciences Massey University P. Bag 11-222 Palmerston North New Zealan

[8] M. Abramowitz, Contrast Methods in Microscopy: Transmitted Light, Olympus America, Inc., Melville, New York, 1987, 31 pp.

[9] J. G. Delly, Photography Through The Microscope. 9e, Eastman Kodak Co. Rochester, New York, 1988, 104 pp.

[10] H. G. Kapitza, Microscopy From The Very Beginning. Carl Zeiss, Oberkochen, Germany, 1994, 40 pp.

[11] J. B. Pawley (ed.), Handbook of Biological Confocal Microscopy, New York: Plenum Press, 1995.

[12] K. R. Spring and S. Inoué, Video Microscopy: The Fundamentals, New York: Plenum Press, 1997.

[13] E.H.K. Stelzer, Practical Limits to Resolution in Fluorescence Light Microscopy, in R. Yuste, F. Lanni, A. Konnerth (eds.), Imaging Neurons: A Laboratory Manual, New York: Cold Spring Harbor Press, 12.1-12.9, 2000

[14] B. Murphy, Fundamentals of Light Microscopy and Electronic Imaging, New York: Wiley-Liss, 2001.

[15] V. Centonze and J. Pawley, Tutorial on Practical Confocal Microscopy and use of the Confocal Test Specimen, in J. B. Pawley (ed.), Handbook of Biological Confocal Microscopy, New York: Plenum Press, 549-570, 1995

[16] M. Born and E. Wolf, Principles of Optics, New York: Cambridge University Press, 1999.

[17] E.H.K. Stelzer, Contrast, Resolution, Pixelation, Dynamic range, and Signal-to-Noise Ratio: Fundamental Limits to Resolution in Fluorescence Light Microscopy, Journal of Microscopy, 189: 15-24, 1997.

[18] J. Pawley, Fundamental Limits in Confocal Microscopy, in J. B.Pawley (ed.), Handbook of Biological Confocal Microscopy, New York: Plenum Press, 19-37, 1995.

[19] R. H. Webb and C. K. Dorey, The Pixelated Image, in J. B. Pawley (ed.), Handbook of Biological Confocal Microscopy, New York: Plenum Press, 55-67, 1995.

[20] J. E.N. Jonkman and E. H. K. Stelzer, Resolution and Contrast in Confocal and Two-Photon Microscopy, in A. Diaspro (ed.), Confocal and Two-Photon Microscopy: Foundations, Applications, and Advances, New York: Wiley-Liss, 101-125, 2002.

[21] Hell S and Stelzer E H K 1992 Fundamental improvement of resolution with a 4Pi-confocal fluorescence microscope using two-photon excitation Opt. Commun. 93 277–82

[22] Van Der Voort H T M and Brakenhoff G J 1990 3D image formation in high-aperture fluorescence confocal microscopy: a numerical analysis J. Microscopy 158 43–54

[23] Optical Coherence Tomography: System Design and Noise Analysis, Michael H. Frosz, Michael Juhl ,Morten H. Lang, Risø National Laboratory, Roskilde, Denmark, July 2001

[24] Laser Scanning confocal Microscopy, Nathan S. Claxton, Thomas J. Fellers, and Michael W. Davidson, Department of Optical Microscopy and Digital Imaging, National High Magnetic Field Laboratory, The Florida State University

[25] Sheppard C J R 1988 Aberrations in high aperture conventional and confocal imaging systems Appl. Opt. 27 4782–6

[26] Hell S, Reiner G, Cremer C and Stelzer E H K 1993 Aberrations in confocal fluorescence microscopy induced by mismatches in refractive index J. Microscopy 169 391–405

[27] Lord Rayliegh Scientific Papers vol III, p 436

[28] Michelson A A 1927 Studies in Optics (Chicago, IL: University Chicago Press)

[29] Sandisson D R and Webb W W 1994 Background rejection and signal-to-noise optimization in confocal and alternative fluorescence microscopes Appl. Opt. 33 603–15

[30] Three-Dimensional Surface Measurement Confocal Scanning Microscope , D.K. Hamilton and T. Wilson University of Oxford, Department of Engineering Science, Parks Road, Oxford

[31] The design and construction of a cost-efficient confocal laser scanning microscope, Peng Xia and Bartlomiej Rajwa*Purdue University Cytometry Laboratories, Bindley Bioscience Center, Purdue University, West Lafayette, Indiana 47907,* James T. Jones and J. Paul Robinson, *Weldon School of Biomedical Engineering, Purdue University, West Lafayette, Indiana 47907,* Received 2 July 2006; accepted 13 October 2006

APPENDICES

A. THE POINT-SPREAD FUCNTION

In three (scaled) dimensions the amplitude diffraction pattern for intensity taken from Richards and Wolf [3] is found by using an electromagnetic wave falling on a (pin)hole as a source for the field at the point ρ,ς,φ Figure A1 shows the axes and the notations. The electric and magnetic field components in the directions ρ,ς and φ are [2]

Where $\varphi = 0$ is the direction of the source polarization, A is a scaling constant, and

$$e(\rho,\varsigma,\varphi) = -iA(I_0 + I_2)\cos\varphi\hat{r} - iA(I_0 - I_2)\sin\varphi\hat{j} - 2AI_1\cos\varphi\hat{z} \qquad \text{(A.1)}$$

$$h(\rho,\varsigma,\varphi) = -iA(I_0 + I_2)\sin\varphi\hat{r} - iA(I_0 - I_2)\sin\varphi\hat{j} - 2AI_1\sin\varphi\hat{z} \qquad \text{(A.2)}$$

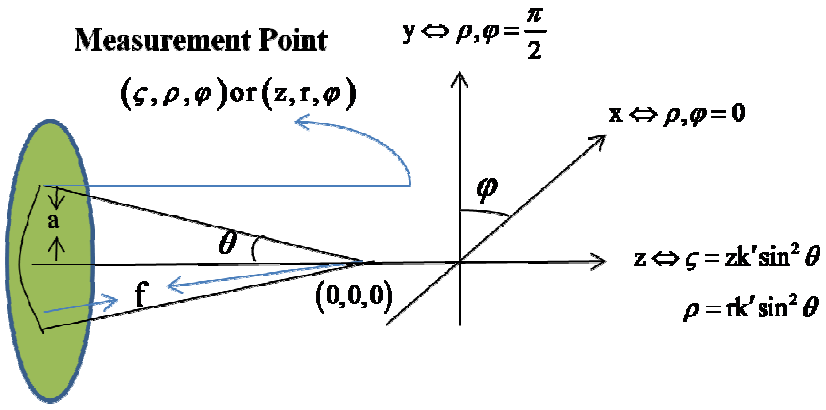

FigureA1. The psf is measured at the point (ρ,ς,φ) or (z,r,φ) when the focus is at the origin and the integration is carried out over the points of the wavefront in the pupil.

$$I_0(\varsigma,\rho)=\int_0^{\nu} j_0(p\sin\alpha/\sin\nu)\sqrt{\cos\alpha}\sin\alpha(1+\cos\alpha)e^{i\varsigma\cos\alpha/\sin^2\nu}d\alpha \tag{A.3}$$

$$I_1(\varsigma,\rho)=\int_0^{\nu} j_1(p\sin\alpha/\sin\nu)\sqrt{\cos\alpha}\sin^2\alpha e^{i\varsigma\cos\alpha/\sin^2\nu}d\alpha \tag{A.4}$$

$$I_2(\varsigma,\rho)=\int_0^{\nu} j_2(p\sin\alpha/\sin\nu)\sqrt{\cos\alpha}\sin\alpha(1-\cos\alpha)e^{i\varsigma\cos\alpha/\sin^2\nu}d\alpha \tag{A.5}$$

Since $I_1(\varsigma,0)=I_2(\varsigma,0)=0$, here $\sin\nu=\frac{NA}{n}$, by using this simplification in equations(3) and (4), we can get the fallowing simplified equation

$$I_0(z,r)=\int_0^{\nu} j_0(rk'\sin\alpha)\sqrt{\cos\alpha}\sin\alpha(1+\cos\alpha)e^{izk'\cos\alpha}d\alpha \tag{A.6}$$

$$I_1(z,r)=\int_0^{\nu} j_1(rk'\sin\alpha)\sqrt{\cos\alpha}\sin^2\alpha e^{izk'\cos\alpha}d\alpha$$

(A.7)

$$I_2(z,r)=\int_0^{\nu} j_2(rk'\sin\alpha)\sqrt{\cos\alpha}\sin\alpha(1-\cos\alpha)e^{izk'\cos\alpha}d\alpha \tag{A.8}$$

The point spread function for intensity is then simply $e\cdot e^*+h\cdot h^*$, for

$$p(\varsigma,\rho)=\left\{|I_0|^2+2|I_1|^2+|I_2|^2\right\} \tag{A.9}$$

Where we assume normalization to make various scale factors equal 1. When phase orpolarization matter the amplitude psf of equation (A1) must be used.In the confocal case,

$$p_{confocal}(\varsigma,\rho)=\left\{|I_0|^2+2|I_1|^2+|I_2|^2\right\} \tag{A.10}$$

B. THE MATLAB CODE

I have written a simple code in Matlab 8.6 to plot the graph of the datas which I have taken by the main program in LabView7.1. The fallowing code plots the 3-D graph of the file *data.txt*

```
clear all
load data.txt;
rawdata = data;
x = rawdata(:,1);
y = rawdata(:,2);
data = rawdata(:,3:end);
c1 = size(data);
c2 = c1(2);
y = y(1:c2);
figure(2)
M = surf(y,x,data);
shading interp
colormap(bone)
```